AIMS Energy, 13(6): 1463–1517.
DOI: 10.3934/energy.2025055
Received: 16 July 2025
Revised: 01 October 2025
Accepted: 31 October 2025
Published: 09 December 2025

https://www.aimspress.com/journal/energy

Review

Potential of high entropy alloys in hydrogen storage technologies

Adebayo Olutumbi Ogunyinka[1,*], Abimbola Patricia Idowu Popoola[1], Sisa Lesley Pityana[2], Emmanuel Rotimi Sadiku[1], Olawale Mohammed Popoola[3] and Modupeola Oluwaseun Dada[1]

[1] Department of Chemical, Metallurgical and Materials Engineering, Tshwane University of Technology, Pretoria, South Africa
[2] Council for Scientific and Industrial Research (CSIR) Pretoria, South Africa
[3] Centre for Energy and Electric Power, Tshwane University of Technology, Pretoria, South Africa

* **Correspondence:** Email: adebayo2602@gmail.com; Tel: +27749574567.

Abstract: The importance of hydrogen in economic development can be attributed to its great potential as a clean and renewable energy source. The structural versatility of metal hydrides has proven to be instrumental in the design of hydrogen storage components. Despite its low volumetric energy density and light in nature, its storage remains challenging due to its high susceptibility to evaporation. However, hydrogen desorption-absorption from a convectional metal hydride can be challenging to gravimetric storage. The lack of effective materials with the potential of reversibility and heat transfer also contribute to these issues. Therefore, researchers continue to explore strategies to mitigate the drawbacks associated with metal hydrides by developing advanced materials such as high-entropy alloys (HEAs) with improved reaction kinetics and finding ways to enhance their practical utility for various applications. HEAs have unique compositional flexibility and diffusion properties, making them efficient for hydrogen storage without high pressure and extremely low-temperature requirements. In this review, we focused on the design and synthesis strategies of HEA alloys, the thermodynamics of HEA for hydrogen storage, the thermal analysis of hydrogenation in HEAs, and the embrittlement of structural alloys in the presence of hydrogen. The review indicated that HEAs have the potential to improve the properties of solid-state storage materials significantly. Their efficiency and compatibility with fuel cells make them a promising candidate for the future of sustainable energy.

Keywords: high-entropy alloys; hydrogen storage; metal hydride; absorption; desorption

Abbreviations: *Mfit*: heterogeneous strain of misfit atoms; *yi*: atomic radius; *Kj*: atomic percentage; J_{th}: alloys component; t: time; $\bar{c}$: constant term; Z: position in z-direction; A: amplitude of the sinusoidal variation; μ_H: hydrogen chemical potential; C_H: compositional variable; ${}^{conf}G_m^{\emptyset}$: physical parameter; $B_y^{\emptyset}$: molar fraction for each phase; λ: wavelength; C: mean composition concentration of substance; e: euler's number, a numerical constant; D: diffusion coefficient; $\frac{S}{k}$: entropy factor; $E(H_2)$: energy of the isolated H_2 molecule; ΔG_{ads}: Gibbs free energy of adsorption; Ɛ: emissivity of hydrogen; $\dot{m}$: mass flow rate; L: latent heat of the phase of the composition material; μ: dynamic viscosity of hydrogen gas; K^o: atmospheric pressure; K_{H2}: hhydrogen gas pressure in the atmosphere; v: hydrogen flow rate; E_{H_2}: energy of a hydrogen molecule; E_{system}: total energy of the substrate with the adsorbate; $E_{substrate}$: total energy of the clean substrate without adsorbate; ΔH: enthalpy; ΔS: entropy; ΔG: Gibbs free energy; G_m: molar Gibb energy of phase $\emptyset$; Tn: melting temperature (T^oC); $n^{\emptyset}$: number of moles; R: gas molar constant; P_p: plateau pressure; P^o: standard pressure (1atmospheric); Peq: pressure equilibrium at atmospheric pressure; C_p: specific heat capacity; ρ: density of the fluid or gas; A: surface area; v: H_2 flow rate; Q: Heat sources; Δρ system: electron charge distribution of the system; ρ_s: electron charge of substrate; $E_{total}(M)$: energy of the HEA without hydrogen; (ΔE_{ZPE}): zero-point energy; E: thermal conductivity; Ea: activation energy; $\frac{\delta T}{\delta x}$: temperature gradient; S_r, Sz: pressure drops of hydrogen gas; $\Delta G^{(BH\alpha)}$, $\Delta G^{(BH\beta)}$, $\Delta G^{(BH\theta)}$: Gibbs free energy of hydride in α, β, and θ phases; H^{H_2}: standard enthalpy; S^{H_2}: entropy of the hydrogen; n_m: mole numbers of metal atoms; n_H: mole numbers of hydrogen; E_{total} (MH_2): total energy of hydrogen in metal; $E_{adsorbate}$: total energy of the isolated adsorbate

1. Introduction

With the rising energy cost and the need for sustainable energy solutions, researchers are actively exploring advanced materials and optimizing their composition for efficient storage. Among these materials are intermetallic alloys, which include AB intermetallic compounds (such as AB_2, and AB_5) and HEAs [1–3]. This intermetallic compound consists of two elements labeled A and B in a specific stoichiometric ratio as AB_x (A is rare earth metals; B is a transition metal; $2 < x < 5$). These alloys have the potential to absorb and release hydrogen efficiently, and they are good for hydrogen storage applications. A is a metal that easily forms hydride (such as Ti, V, Zr, and Y), while B is a non-hydride-forming metal (such as Cr, Mn, and Fe). The typical examples of these compositions are AB-alloys (TiFe), AB_2-alloys ($TiMn_2$ and TiFe), and AB_5-alloys ($LaNi_5$).

The AB_2 alloy has the promising capability of forming new phases at high pressure; nevertheless, impurities in the hydrogen environment and the high cost of rare-metal alloys limit their applications in energy storage [4]. Similarly, AB_5 alloys have attractive properties for hydrogen storage, such as low activation energy and pyrophoricity, high intrinsic kinetics, and the ability to substitute various A

and B elements into their lattice sites. The production of these alloys is complex and requires an adequate vacuum environment due to their reactivity and high melting temperatures. Nonetheless, it faces the challenges of activation, purification, and high-pressure concentration isotherm (PCT) instability [5,6]. A possible cause is pressure composition hysteresis (Figure 1), which can lead to unstable conditions for hydrogen absorption and desorption. In hydride formation, hysteresis can also cause loss of thermodynamic efficiency during the thermal cycle, thus impacting the energy balance of hydrogen storage systems [7]. In hydrogenated HEAs, a notable hysteresis effect is observed within the region of the pressure-composition isotherm (PCI) profile where a two-phase alloy structure is present. This effect is controlled by elastic strain and interfacial energy [8–10].

The difference in pressure required for hydrogen absorption and desorption in HEAs can be attributed to several factors (elastic changes, diffusion barriers, and microstructural changes). The alloy forms a hydride phase at a relatively high pressure due to the energy required to overcome the initial energy barrier for hydrogen atoms to occupy interstitial sites. However, a lower pressure is required to break down the hydride back to metal in HEA. As such, the lag creates a hysteresis loop [11]. The energy dissipated in the loop will manifest as irreversible losses, thereby reducing the usable hydrogen capacity and increasing energy consumption in storage systems [12]. A hysteresis effect can also cause uneven expansion and contraction of the alloy lattice, leading to stress accumulation and mechanical degradation.

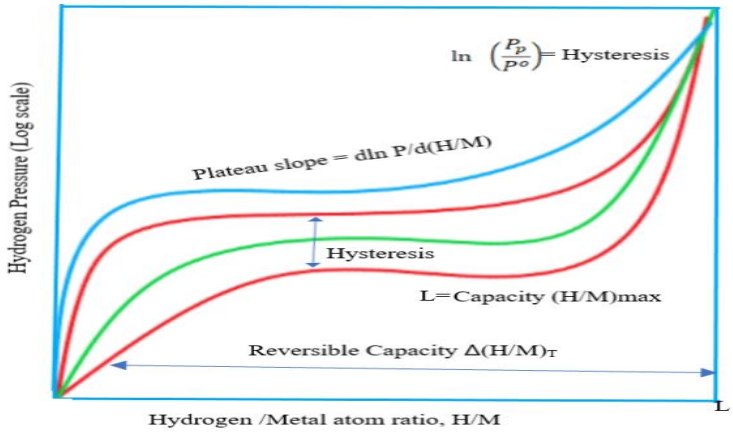

Figure 1. Depicting hysteresis in a hydrogenated HEA, in the region of the PCI profile where the two-phase alloy co-exists, absorption pressures tend to exhibit a hysteresis effect.

Lu, et al.[13] explored TiVNbCrMo HEAs for hydrogen storage. The study involved experimental analysis where HEA samples underwent a two-hour evacuation process at a temperature of 673 K (Figure 2). Each sample was tested at 300 K for ~100 s under high pressure (above 0.1 MPa). Maximum hydrogen equilibria were achieved in the alloys Mo_2, Mo_4, and Mo_6, with values of 3.57, 3.53, and 3.21 wt.%, respectively.

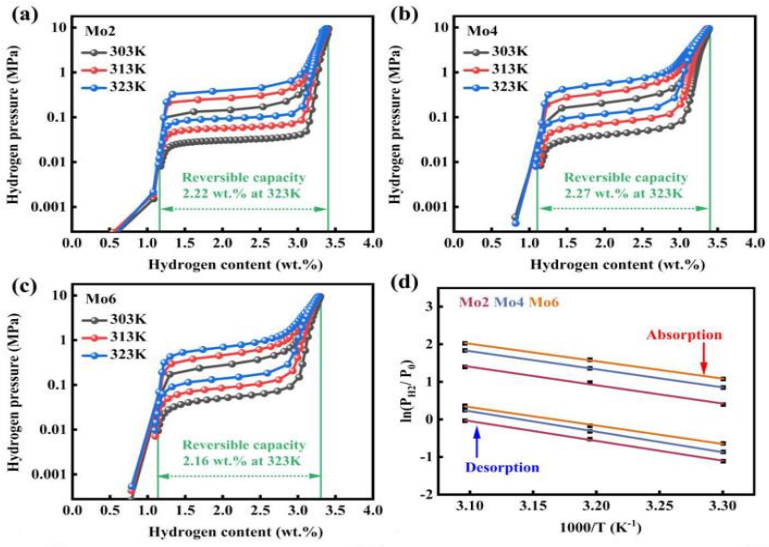

Figure 2. Experimental pressure composition temperature (PCT) isothermal curves were obtained for TiVNbCrMo (HEAs) at various temperatures. PCT measurements (a) at 303 K represent only absorption. In contrast, the PCT curves (b and c) were measured at 313 K and 323 K, encompassing both absorption and desorption processes, while (d) represents the Van't Hoff plot [13].

In this research, we compared the experimental results against the theoretical PCT plot of TiZrNbVMoCr HEA. The PCT (Figure 3a) plot was measured at a temperature of 25 °C (298 K) for only absorption and at 50 °C (323 K) and 500 °C (773 K) for both absorption and desorption. These varying temperatures provide a comprehensive understanding of the HEAs' hydrogen storage capabilities under different conditions. The Van't Hoff plot for hydrogen absorption and desorption (Figure 3b) displays two distinct lines, where each represents a different phase transformation plateau. The absorption line present is the α-β plateau, which is an equilibrium between the alpha (α) and beta (β), thus reflecting the solid solution and the beta (β) hydride phases, while the desorption line β-δ plateau represents the equilibrium between the beta (β) hydride phase and the delta (δ) hydride phase. The magnitude of the slope is proportional to the enthalpy change. The β-δ plateau has a more negative enthalpy change than that of the α-β transition. This indicates that δ hydride is a more energetically favorable process.

Figure 4a illustrates PCT curves for AlTiZrNbVCr HEA that occur at various temperatures, exhibiting similar shapes indicative of a typical hydrogen absorption plateau in BCC alloys. This plateau signifies a two-phase region where hydrogen absorption occurs at near-constant pressure, thus reflecting stable hydride formation. The maximum hydrogen storage capacity for AlTiZrNbVCr HEA is 2.75 wt.%. It is an indication of its promising performance as a hydrogen storage material. From the Van't Hoff plot (Figure 4b), the thermodynamic properties (ΔH and ΔS) of the HEA hydride are extracted, which indicate the heat management requirement. The slope of this plot corresponds to the enthalpy (ΔH) of the HEA hydride, indicating the hydrogen absorption and desorption process, while ΔS contributes to overall thermodynamic stability and equilibrium conditions. This information can be used in the designing of a thermal management system.

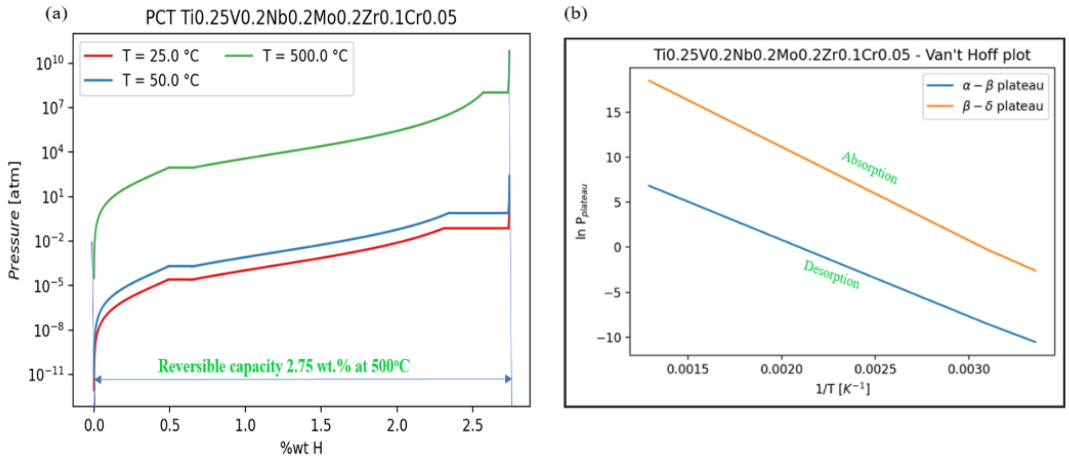

Figure 3. The pressure-composition-temperature isothermal for TiZrNbVMoCr at temperatures 298 K, 323 K, and 773 K.

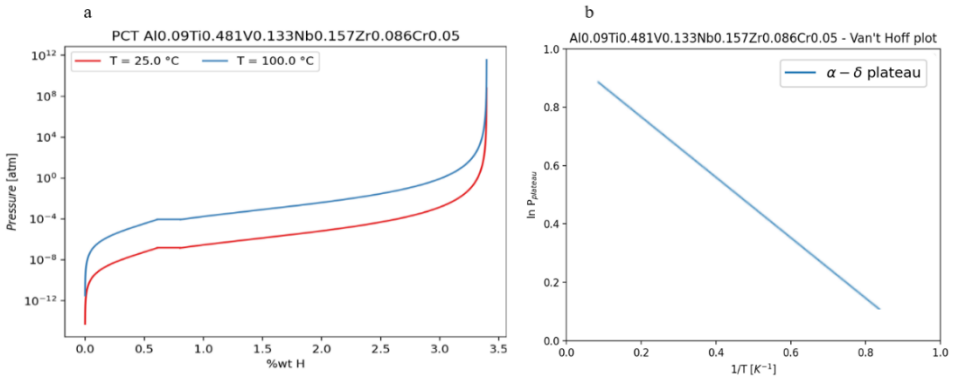

Figure 4. (a) PCT curves under different temperatures and (b) Van't Hoff equation for desorption and absorption.

Generally, intermetallic alloys exhibit hydrogen absorption and desorption capabilities. Many of these intermetallic alloys have been successfully utilized in various industrial processes and applications, demonstrating adequate performance for intended purposes. For instance, NiMH batteries show good performance and can be used in consumer electronics and hybrid vehicles. Similarly, lithium-ion batteries have excellent performance in terms of energy density and are applicable where longevity is required, such as in electric vehicles [14,15]. Additionally, MgH_2 and AB_2 alloys have a high capacity for hydrogen energy storage and are used in many applications, such as fuel cells and hydrogen storage systems. In addition, the standard enthalpy of formation for MgH_2 is −75.2 kJ/mol, which is high enough when compared with VH_2 and PdH_2 [16,17]. The hydrogen PCT properties of AB composition can be modified to enhance their overall energy efficiency. More research is needed to design and develop a cost-effective and efficient intermetallic alloy that are more stable and reversible.

Other materials can be improvised, such as organic and inorganic porous materials: Carbon nanotubes, graphene, fullerenes, metal-organic frameworks (MOFs), covalent organic frameworks,

and polymers, which can perform hydrogen storage [18]. These materials exhibit Van Der Waals force properties, resulting in low binding energies and rapid adsorption kinetics. However, its weak bond characteristic may not be suitable for ambient temperature and elevated pressure to achieve acceptable hydrogen storage capacity. Other limiting factors include porous blockage, pore size distribution, and complex synthesis. Therefore, there is a need to address these issues; doping these materials with other elements is a new strategy to enhance hydrogen storage capacity. For instance, lithium-doped boron benzene/graphene structures have demonstrated hydrogen capacity as high as 13.7 wt.%, thereby leveraging the strong interaction between lithium sites and hydrogen [19]. Certain MOFs doped or optimized at a low temperature (approximately 77 K) can achieve a capacity around 7.49 wt.%, benefitting from their high porosity and tailored binding sites to optimize hydrogen [20].

Additionally, HEA materials have become increasingly important in hydrogen storage. This is because of its high capacity for hydrogen storage, fast kinetics of absorption and desorption, and efficient cycle stability. Also, the properties of HEAs such as high melting point, a disordered structure and strained lattice distortion aid in effective hydrogen storage. Therefore, the synthesis of HEAs could be a solution to address the challenges faced by AB alloys in terms of reversibility under varied conditions. An improved functionality of HEAs has been achieved through the optimization of their alloy composition, temperature, and pressure. However, the complexity of the microstructure of HEAs could hinder their practical applications [16,21]. As research progresses, developing innovative techniques such as Additive Manufacturing (AM) and optimizing existing methods to enhance the properties and performance of HEAs [22,23] could be the solution. Likewise, understanding HEAs at the microstructural and atomic level could also provide a solution to the above challenges [24].

2. The Design of HEA alloys, synthesis, and potential applications

2.1. Design of HEA alloys

The design of new alloys involves computational tools and high-throughput experimentation that explores vast combinations of elements. This approach has revolutionized the field of materials science in recent years. These alloys are typically formed by mixing various metallic elements in equal or nearly equiatomic proportions [25]. These metallic elements are combined stoichiometrically and as such, forming a homogeneous mixture with a uniform crystal structure poses some challenges. Some degree of atomic disorder is caused by the presence of different elements that consequently affects the crystal lattice. These mixings favor the formation of a single solid solution, whose concentration ranges between 5 and 35%. Figure 5, illustrates the composition of metallic elements in HEAs, and showcasing their random solution structure.

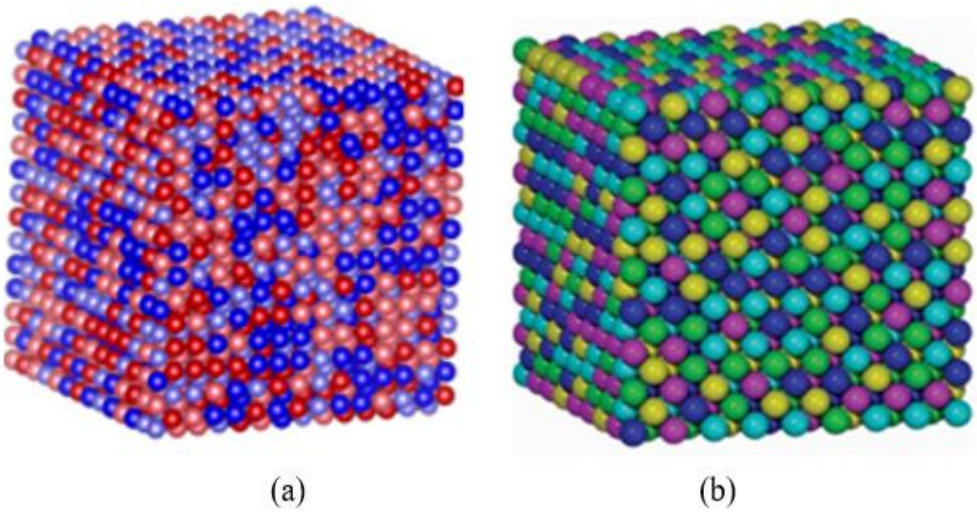

Figure 5. The composition of metallic elements in HEAs [26,27].

Moreover, lattice distortion can produce heterogenous and homogenous strains that will affect the properties of HEAs [21]. The heterogenous strain usually occurs due to the effect of misfit atoms in HEAs. Consequently, this impacts the mechanical and physical properties of alloys. The heterogeneous strain of misfit atoms, *Mfit*, is given in Eq 1 [28,29].

$$Mfit = \sqrt{\sum_{i=1}^{n} K_j \left(1 - \frac{y_i}{\sum_{j=1}^{n} K_j y_j}\right)^2} \quad (1)$$

where y_i denotes the atomic radius and K_j is the atomic percentage of the jth component.

Several heterogeneous strain methods can show some variation in strain across a material; an X-ray diffraction microscope (XRD) can reveal such variations by examining regions of the crystal [30]. For instance, if a crystal experiences non-uniform stress, XRD can detect strain differences between its surface and interior. Using this technique, one can study crystalline structure. Unlike XRD, the transmission electron microscope (TEM) can use a beam of electrons to visualize the internal structure of materials at a very high resolution, down to the atomic scale. As such, it provides information about the crystal structures, defect grain boundaries, and nanoscale features [31]. Unlike heterogeneous strain methods, with the homogenization of solid solutions, many structural phases will be distributed evenly. Since HEAs are designed to have high configurational entropy due to the random mixing of multiple elements at the atomic scale, this randomness may result in a disordered atomic arrangement where atoms of different elements are distributed through the entire crystal lattice [32,33]. There are many effects this uniform distribution of elements can cause, especially in HEAs: (i) It can suppress phase segregation, and (ii) it can form intermetallic compounds that degrade the alloys performance [5,34]. In addition, chemical segregation usually occurs on a microscopic scale and can influence stability. Removal of micro-segregation through solid-state diffusion processes can be challenging as a uniformly distributed and well-defined solute will decay at a micro-segregation rate over time. Therefore, to mitigate this effect homogenization is required [35,36]. Equation 2 showed the homogenization of a solid solution system. As homogenization progresses, alloying elements begin

to diffuse, and this causes changes in the composition profile. The elements in a solid solution were observed to be distributed evenly. In this case, material properties were predicted consistently across the volume.

$$C\{z,0\}=\bar{c} + \mathrm{A}\sin\frac{\pi z}{\lambda}\ , \tag{2}$$

$$C\{z,0\}= \bar{c} + \mathrm{A}\sin\frac{\pi z}{\lambda}\ e^{-\frac{\bar{D}t\pi^2}{\lambda}}, \tag{3}$$

$$\text{Therefore, } \lambda = 4\tau\pi^2\mathrm{G} \tag{4}$$

The initial concentration distribution is shown at time t = 0. It consists of a constant term $\bar{c}$ and a sinusoidal term $\mathrm{A}\sin\frac{\pi z}{\lambda}$, that varies with position z, which is the spatial coordinate. A, denotes the amplitude of the sinusoidal variation, and λ is the wavelength of this variation. C represents the mean composition of the substance (hydrogen gas H_2) being diffused. From the initial condition (as described in Eq 3), it outlines the dynamics of how the composition of hydrogen gas (H_2) changes over time during the diffusion process. The exponential term $e^{-\frac{\bar{D}t\pi^2}{\lambda}}$, accounts for the decay of the concentration over time due to diffusion. 'e' is a numerical constant called the Euler's number, otherwise known as the Napier constant, whose value is the initial amplitude of the waves (e = 2.71828) while τ is a characteristic time scale that is actually equivalent to (1/e = 0.3678796886). Moreover, D_t represents a constant diffusion coefficient. This Eq 3 defines the wavelength λ in terms of other parameters, where τ indicates a characteristic time scale and is the inter-diffusion coefficient.

2.2. Computational tools

The computational tool has significant roles in creating, measuring, and computing models for alloy compositions in terms of crystal structures and phase diagrams, especially for multinary systems. In this process, an electronic calculation machine that solved a pertinent equation rapidly was employed [37]. The main approach of this computation is to interlink process, structure, properties, and performance, which are the core of materials science [31]. The combination of these tools with material development will unify the design and manufacturing processes. This strategy has resulted in numerous successful multicomponent materials with an optimal balance of engineering properties. The potential of using the tools lies in their capability to describe complex patterns and the availability of resources, either from experiments or computations [38]. Various methods of using computational tools, such as machine learning algorithms, molecular dynamics simulations, and density functional theory calculations, have been employed to predict the properties of new entropy alloys before they are synthesized. These tools would provide insights into the atomic-scale structure and behavior of the alloy (mechanical, thermal, and electronic properties). Figure 6 illustrates stages of HEA alloy preparation, from design and synthesis to the final application. This iterative process enables the tailoring of HEAs to meet specific structural-performance requirements in diverse applications.

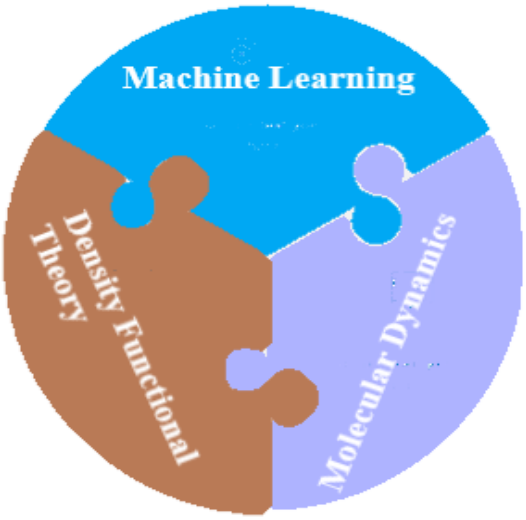

Figure 6. Computational tools.

2.2.1. Machine learning

Machine learning (ML) is very crucial in alloy design; its application is enormous, especially in establishing some relationships in the alloy parameters (composition, microstructure, and properties). This model uses a variety of algorithms, such as linear regression, random forest, and neutral networks. Each of these algorithms was created to predict and perform different functions depending on the nature of the dataset and the specific properties required [39]. For example, a random forest algorithm is appropriate when the relationships between alloy composition and properties are complex and nonlinear. As a result, it can handle a wide range of features, while the neutral network is highly flexible and capable of capturing intricate patterns. The ML can predict the density, hardness, and strength of hydrogenated HEAs based on their composition and processing parameters [40]. HEA features may generally fall into the following categories of environmental descriptors (relative humidity, corrosion, and oxidation). For instance, looking at properties, it may not be strength only but a strength under irradiation that needs to be featured. The use of the Gaussian Process Regression (GPR) model is a typical example, and it is a significant asset in materials science, particularly for predicting properties such as hydrogen storage enthalpy in HEAs. The genuineness of this approach is underscored by experimental validations of GPR predictions. For example, the confirmed reversible room temperature hydrogen storage in $Ti_xZr_{2-x}CrMnFeNi$ HEA (x = 0.5, 1.0, 1.5). This highlights the effectiveness and reliability of GPR in guiding materials research and development [41].

2.2.2. Molecular dynamics

Molecular dynamics (MD) has the potential to explore molecular behavior and atomic properties [42]. It uses Lagrangian, Hamiltonian, and Newtonian functions for modeling special features and properties of materials such as heat capacity and thermal conductivity [43]. MD is applicable in investigating the role of defects (vacancies and dislocations) that influence hydrogen absorption. It can be used to study stress evolution and changes in mechanical behavior during hydrogen absorption and desorption. By using parallelization techniques to scale up the MD model,

the storage performance of HEAs will improve greatly, especially when dealing with large-scale systems that involve hydrogen storage. A model based on atomic descriptors is relevant in this simulation as they can be used to estimate elastic constants in HEAs, particularly where stress-strain analysis is required to determine the elastic modulus [44].

Similarly, DFT and MD simulations are employed to predict hydrogen binding energy and absorption sites within HEA lattice structures. A notable instance of this is the prediction and subsequent experimental validation involving TiVNbCrMo HEAs, which effectively demonstrates the real-world utility of DFT and MD methodologies in the field of materials science. These computational techniques offer valuable insights into material properties, guiding the development and optimization of HEAs for hydrogen storage and other applications [45].

2.2.3. Density functional theory calculations

The simulation of HEAs-hydride requires high-performance computing. In this case, a Density Functional Theory (DFT) model is required to study the changes in electronic structure associated with hydrogen absorption in HEAs [46]. Using the DFT algorithm (Hamilton) to determine adsorption energy and identify a favorable site for hydrogen absorption and desorption [47]. Zhang, et al. [48] explored the DFT simulation to assess the phase formation and stability of HEAs. The integration of this model with thermodynamics will provide detailed information on hydrogen absorption in HEAs.

The lattice distortion in HEA often alters the atomic spacing and electronic structure. In this case, the distorted lattice sites produce heterogenous interstitial volumes and bonding environments where hydrogen atoms can occupy and migrate. As such, it changes the local potential energy barriers (for hydrogen atoms) that need to be overcome in order to hop from one interstitial site to another. These distortions often generate an intrinsic stress field, thereby leading to a complex energy landscape at the atomic level. DFT calculations are widely used to compute adsorption energies because they provide accurate quantum mechanical total energies of atomic systems [49,50]. The adsorption energy E_{adsorp} is defined as

$$E_{adsorb} = E_{system} - (E_{Substrate} + E_{adsorbate}) \tag{5}$$

Adsorption energy difference $\Delta E_{adsorb} = E'_{adsorb} - E_{adsorb}$.

Moreover, the distorted lattice interacts with the hydrogen dislocation mechanism, affecting trapping and emission of hydrogen atoms. Introducing a hydrogen atom at an interstitial site, the equation for adsorption energy can be written as:

$$E_{adsorb} = E_{HEA+H} - E_{HEA} - \frac{1}{2}E_{H_2}, \tag{6}$$

$$\Delta E_{adsorb} = E'_{adsorb} - E_{adsorb}$$

where E_{H_2} represent energy of a hydrogen molecule.

Charge density difference $\Delta\rho$ plots can be obtained by subtracting the total charge of the system from individual charges of the substrate and adsorbate.

$$\Delta\rho_{system} = \rho_{substrate} + \rho_{adsorbate}, \tag{7}$$

where $\Delta\rho$ system represent electron charge distribution of the system, ρa and ρs indicates an electron charge of adsorbate and substrate respectively.

Additionally, the differential Gibbs free energy of adsorption ΔG_{ads} for the different surfaces were calculated using the DFT total energy, corrected by the entropic change ($T\Delta S$) and the difference in zero-point energy (ΔE_{ZPE}) derived from the vibrational frequencies.

$$\Delta G_{ads} = \Delta E_{adsorb} + \Delta E_{ZPE} - T\Delta S, \quad (8)$$

For instance, the hydrogen binding energy E_B is the energy in the TiZrHfMoNb HEA hydrides.

$$E_B = \frac{1}{n}\left[E_{total}(M) + \frac{n}{2} E(H_2) - E_{total}(MH_n)\right], \quad (9)$$

$E(H_2)$ denotes energy of the isolated H_2 molecule, $E_{total}(MH_2)$ indicate total energy of hydrogen in metal, while E_{total} (M) described the energy of the HEA without hydrogen.

By this definition, the more positive the binding energy is, the stronger the interaction between hydrogen and HEA [51].

The DFT simulation is also applicable for high-throughput screening for a wide range of HEA, thus leading to the development of new alloys [52]. The use of a linear-response algorithm is crucial in the DFT as it will help in computing the microstructure and shear modulus [53]. For example, if the hardness property of a hydrogen storage is required, the melting temperature of the alloy will be used to indirectly determine the bond strength [54]. In summary, the choice of algorithm will depend on the nature of the data, the problem at hand, and the specific requirements of the task.

2.3. Synthesis of HEAs

The synthesis of HEAs requires a systematic approach to achieve the desired balance of elements and properties. Numerous studies have been carried out to explore and optimize the synthesis methods of HEAs. The aim is to improve the efficiency, scalability, and control of the synthesis process to further advance the development application. A continuous exploration of new composition and synthesis methods will push the boundaries of alloy development [55–57].

The synthesis of HEAs may require accurate control of compositional mixing to achieve a homogenous solid solution and stable phases. However, due to the demanding nature of the processes involved, which require the use of high temperatures and rapid cooling. Current methods often rely on batch processing or complex setup that limits continuous, large-scale production. For example, while plasma jets offer certain advantages, their economic scalability becomes a major obstacle. These limitations necessitate exploring alternative approaches that can overcome these bottlenecks and enable more efficient and cost-effective production processes [58].

The particle size distribution has a significant effect on the processability of additive manufacturing, which operates within the size limits of 10–45, 45–106, and 20–200 um, respectively. Achieving particle size uniform distribution and composition in a nanoparticle or thin film may be difficult in a continuous industrial process. High energy consumption as a result of extreme temperatures, such as in plasma jets and rapid quenching, increases the cost of production [59].

The cost implications for industrial sectors are significant, as numerous synthesis methods often necessitate the use of precious metals or pre-alloyed powder and costly equipment, such as atomic layer deposition and plasma reactors, thereby increasing the overall financial burden on industrial operations.

There are techniques that involve various processing routes, which start with material selection,

compositional design, material preparation, and processing. This selection will be exposed to material processes such as mechanical alloying, arc-melting, additive manufacturing, and casting. In this case, the materials will be heated to a high temperature to produce liquid metal [60]. Nevertheless, the specific steps in this synthesis can vary depending on the type of alloy being produced, the intended application, and the desired properties. Many factors affect the stability of HEA synthesis (Table 1), including its crystal structure, the degree of chemical ordering, and the presence of intermetallic compounds [61]. For instance, the face-centered cubic (FCC) crystal phase is widely used in HEAs as it is highly stable and ductile. A high level of chemical ordering can stabilize the alloy structure and prevent the formation of undesirable phases.

Table 1. The design of alloys, synthesis, and potential applications of HEA [33].

Compositional tools	Properties optimization	Heat treatment	Application	Synthesis method	Cost	Scalability challenges
Phase diagram prediction	Composition refinement. altering the condition of heat treatment	Eliminating defect, homogenizing the alloys, induce the desirable phase transformation	Aerospace, energy storage, and structural materials	Arc melting Additive manufacturing, Casting, mechanical alloying, ball milling, radio frequency magnetron	Energy intensive High purity raw material Specialized equipment	Ingot size High cost of equipment Compositional homogeneity

The presence of intermetallic compounds can affect the stability of HEAs as they can act as nucleation sites for the formation of new phases. Understanding the factors that affect crystal stability is essential to designing and synthesizing new high-performance alloys with unique properties, as buttressed in Eqs (10,11) [62].

$$D = \frac{KT}{h} \exp\left(\{\frac{S}{k}\} \exp - \frac{H}{kT}\right). \tag{10}$$

Similarly, the activation enthalpy increases while the frequency factor decreases, as given in

$$D = \frac{KT}{h} \exp\left(-\frac{H-TS}{kT}\right), \tag{11}$$

where ΔH and ΔS represents the enthalpy and entropy of the system respectively. Additionally, $\frac{H}{kT}$ and $\frac{KT}{h}$ denote the activation enthalpy and the frequency factor**.** Besides, D, and $\frac{S}{k}$, represent the diffusion coefficient and entropy factor, whereas T and K are given as temperature and Boltzmann constant, respectively.

Other factors that influence the thermal stability and elastic properties of this alloy are lattice vibrations. For example, at elevated temperatures, the atoms in a material vibrate more vigorously, causing the HEAs to expand or contract, thus affecting their mechanical properties [63].

Similarly, in the development of high-entropy alloy-hydride (HEAs-h) for hydrogen storage, the design of the material structure is vital to its usage and applications. To this end, Eq (6) refers to the

importance of achieving a homogeneous structure at the melting temperature (*Tn*). This phenomenon will ensure that hydrogen storage performs at an optimal capacity. The homogenous melting temperature of HEAs is given in Eq (12).

$$T_{\mathrm{n}} = \frac{\sum_{\mathrm{j=1}}^{\mathrm{m-1}} \sum_{\mathrm{i=1}}^{\mathrm{m}} \mathrm{T_{i-j}}\{\mathrm{c_i{:}c_j}\}\mathrm{c_i c_j}}{\sum_{\mathrm{i=1}}^{\mathrm{m-1}} \sum_{\mathrm{j=1}}^{\mathrm{m}} \mathrm{C_j C_{i-j}}} \text{ for i} \neq \text{j}, \tag{12}$$

where T_n denotes the homogenous melting temperature, Ci and C_j represent the concentrations of each element, while Ti and T_j indicate the melting temperature of each element, respectively.

The expression in (10–12) describes how the hydrogen atom moves via the alloy's lattice structure in HEAs. The complexity of these multicomponent alloys creates a heterogeneous atomic environment that affects the diffusion pathways [64]. The diffusion coefficient (D) indicates how fast a hydrogen can permeate, which is required for the charging and discharging rate of hydrogen storage. For instance, a slow diffusion rate can lead to an increase in hydrogen trapping atoms in the lattice; as such, it influences storage capacity but potentially reduces the release rate [64,65].

2.3.1 Optimizing the structure and properties of HEAs

Numerous techniques have been developed to improve the structure and properties of HEAs at both cryogenic and elevated temperatures [66,67]. This technique includes alloying additions, controlling the crystal structure, and adjusting the lattice parameters. This process will help mitigate the impact of lattice vibrations and enhance the thermal stability and elastic properties of materials [68]. As part of the technique, composition design will be utilized to select the elements involved. Since each element has a significant role to play, they can influence the crystal structures that form their properties [69]. Consequently, specific crystal structures can also be stabilized, leading to a wide array of special properties, as depicted in Table 2 [70]. Additionally, using a simulation model to predict the crystal structures of HEAs, specific phases with improved properties will be synthesized. Another method is by controlling the grain size using ball milling and mechanical alloying; in this case, a fine grain will produce smooth, equiaxed structural components [71].

Table 2. Factor affecting structure and properties of HEAs.

Alloying additions	Crystal structure control	Lattice parameters
Microstructural control	High throughput	Crystal structure prediction
Selection of elements	Heat treatment and deformation techniques	Mechanical testing
Thermodynamics Modelling	Iterative optimization	Phase diagram and thermodynamics modelling
Compositional design	Grain size control	Computational simulation

Despite attributes obtained through the optimization of the structural properties of HEAs, currently, researchers are exploring the use of refractory high-entropy alloys (RHEAs) for hydrogen storage, particularly the body-centered cubic and body-centered tetragonal (BCC-BCT) structures. These structures exhibit a high level of stability in hydrogen-storage reactions [72]. Besides, BCC structures have larger interstitial sites and more open lattice frameworks, which facilitate higher

hydrogen solubility and faster diffusion rates within the HEAs. This enables improved hydrogen storage capacity and kinetics. The atomic arrangement in BCC alloys enables greater hydrogen-to-metal ratios (H/M), supporting higher hydrogen uptakes than FCC structures, which tend to have denser atomic packing. Typical examples of BCC HEAs include TiVCrFe, TiVCrFeAl, and $TiVNbCr_2$ [73,74]. However, the presence of lave phases in the BCC structure reduces reversibility and pulverization resistance. This may be due to their high degree of chemical bonding and structural complexity. As such, the life cycle of hydrogen storage is limited [75]. Many authors reported that at elevated temperatures, RHEAs undergo phase transformation due to the thermodynamic influence [76]. The synthesis of FCC HEAs for hydrogen storage can be challenging due to the specific structural and chemical properties needed for effective hydrogenation of alloys. The site preference for hydrogen absorption in FCC-HEAs-hydride alloys is complex and sometimes unpredictable [77,78]. In FCC-HEAs-hydride alloys, hydrogen atoms usually occupy octahedral and tetrahedral sites, unlike metal hydride. In fact, it has been shown that hydrogen occupation in both interstices is a complete violation of the Switendick criterion [79]. This means that there is abnormal behavior exhibited by FCC-HEAs hydride, and this is due to an inherent electron decolorization that occurs between the hydrogen atoms and HEAs. Due to this, hydrogens interact less repulsively with each other, and electron localization at octahedral interfaces improves.

Another challenge is that the FCC structure may not be thermally stable under the various conditions in which hydrogen is stored. Unlike other structures, such as BCC, that can offer favorable thermodynamic stability and kinetics for hydrogen absorption and desorption. This is because binding energy for the tetrahedral site usually increases with an increase in hydrogen content and therefore an activation energy barrier that needs to be overcome [80]. Hu, et al. [81] explored HEAs TiZrVMoNb and reported that when the hydrogen contents are below 0.66 wt.%, the FCC hydride becomes thermally unstable at both the tetrahedral and octahedral sites. Similarly, a new HEA TiZrCrMnFeNi was developed capable of absorbing and desorbing hydrogen at room temperature. The behavior of hydrogen in FCC HEAs (CoCrFeMnNi) is highly sensitive to temperature and pressure, as such, any changes in these conditions can influence the solubility and diffusion rate within the FCC lattice, thus affecting the alloys performance [82]. Moreover, ball milling and plastic deformation will increase hydrogen adsorption at room temperature and pressure in FCC-HEAs-hydride alloys. To determine the thermodynamics of a particular alloy system, Gibbs free energy is required. This energy will be estimated using appropriate models and thermodynamic data. These include the enthalpy of mixing, configurational entropy, temperature, and compositional dependence of Gibbs free energy. Once this is computed as described in Eq (8), it can be used to compute the phase diagram for the alloy system, which will reveal the stable phases as a function of temperature and composition. The phase diagram will provide valuable insights into thermal stability behavior and also guide the design of new alloys with improved properties.

In multiphase equilibrium, the molar Gibbs energies for the stable phases are all at a minimum as described in Eqs (13–15) [83].

$$\Delta G_{mix} = \Delta H_{mix} - T\Delta S_{mix}, \tag{13}$$

$$G = \sum_{\emptyset} n^{\emptyset} G_m {}^{\emptyset} a^{n-k}, \tag{14}$$

where n^{φ} is the number of moles and ${}^{\varphi}Gm$ is the molar Gibbs energy of phase φ.

The computational model of hydrogen absorption and desorption was validated through the various experimental data; examples of this analysis are shown in Table 3.

Table 3. Experimentation and theory in thermodynamic analysis [83,84].

Composition	ΔH_{abs}(kJ/molH_2)		ΔS_{abs}(J/KmolH_2)	References
	Experimental Observation	Machine Leaarning		
$Al_{0.05}(TiVNb)_{0.95}$	−52 (±1.5)	−52	−141 (±3)	[83]
TiVNb	−67 (±5)	−58	−157 (±11)	[83]
$Al_{0.10}(TiVNb)_{0.90}$	49 (±1)	−51	−154 (±2)	[83]
$Ti_{0.45}Zr_{0.55}Mn_{0.33}V_{0.45}Ni_{0.85}$	−44.2	−42	−109.1 (±4.8)	[84]

For an ideal solution model for binary alloys, the molar Gibbs energy Gm is written as follows:

$$G_m = \sum x_i\ u_i = \sum x_i\ {}^{o}G_i + RT\sum x_i\ \ln x_i, \tag{15}$$

Furthermore, there is a tendency for this to be obvious if the phases contain sub-lattices. Hence, this is related to different sites of crystal phase structures, especially in disordered solution phases, which are buttressed in Eq (16)

$$^{conf}G_m^{\emptyset} = RT\ \sum_i B_y^{\emptyset} \ln (B_y^{\emptyset}), \tag{16}$$

where R is defined as the gas molar constant, $^{conf}G_m^{\emptyset}$ is the configurational term that describes the contribution of a physical parameter such as magnetism, $B_y^{\emptyset}$ is denoted as a molar fraction of an individual phase.

All constituents occupying the same sub-lattice are mixed, ideally during the configurational term [85]. The above discussions are related to the solubility and phase formation of alloys, which are affected by several factors, including the Hume-Rothery rules, Gibbs phases, intermetallic compounds, and enthalpy. The high degree of solubility achieved in these alloys is attributed to an increase in alloy composition as more phases are formed. Herein, we emphasize the Gibbs phase rule owing to its importance in modeling HEAs thermodynamic properties. The Gibbs phase rule can predict the formation of intermetallic compounds and their stability at equilibrium. At equilibrium, the formation of the intermetallic compound will increase, depending on the enthalpy. Other thermodynamic models, such as the calculation of phase diagrams (CALPHAD) method, can be used to overcome these limitations and provide a more comprehensive understanding of the phase behavior of intermetallic systems [86]. Despite this, intermetallic phase formation that competes with solid solution phases is not fully accounted for in the model, thus limiting the model applications. To strengthen the validity of predicted phase diagrams, it is imperative that high throughput (HT) experimentation be required. Nonetheless, the prediction of metastable phases and transient phases under non-equilibrium limit CALPHAD capability. Therefore, high throughput has the potential to combine synthesis and rapid screening, which will enable fast validation of phase stability across a vast compositional space [87]. Therefore, integration of HT experimental data together with computational CALPHAD workflow will help in improving the accuracy and predictive power for a complex, multi-component HEA. This combined approach will bridge the gap between the predicted equilibrium phases and those obtained during rapid cooling [88].

The relationship between Gibbs free energy for solid solutions and intermetallic formations is expressed in Eq (17)

$$\Delta G^{SS} < \Delta G^{IM} \rightarrow \Delta S^{SS} > \frac{\Delta H^{IM} - \Delta H^{SS}}{T}, \quad (17)$$

where ΔG^{SS} and ΔG^{IM} indicates the Gibbs free energies for both solid solutions and intermetallic formations, ΔH^{SS}, and ΔS^{SS} denote the enthalpy and entropy of solid solutions, while ΔH^{IM} and T stand for intermetallic enthalpy and temperature, respectively.

Furthermore, extensive studies have also reported that a high lattice distortion rate can cause a significant deviation from the ideal crystal structure, which can adversely affect the properties of HEAs. Other factors, such as the concentration of solute atoms and their distribution within the crystal lattice, are also significant in determining hydrogen absorption properties. This was revealed in some of the HEAs, such as CrFeNiTiVZr and CoFeMnTixVZr [89,90]. Eq (18) shows the lattice distortion rate (δ) in HEAs, where M is the atomic number, b_i is the local lattice parameter of the i^{th} atom, and b_0 is the equilibrium lattice constant.

$$\delta = \sqrt{\frac{1}{M}\sum_{i=1}^{M}\left(\frac{b_i - b_0}{(b_0)^2}\right)^2}, \quad (18)$$

The distortion value $\delta < 6.6\%$ is required to form a complete, solid solution. Any distortion greater than this critical value $\delta < 6.6\%$ will lead to the formation of intermetallic precipitation (Laves phase) [91]. Besides, in determining the practical stability threshold for HEAs is challenging due to the complex interplay of factors. For instance, the stability of a single-phase solid solution is enhanced by maximizing the entropy of mixing within the optimal enthalpy ranges. Computational methods, such as ab initio calculations and machine learning, are increasingly used to predict phase stability and explore the relationship between lattice distortion and phase stability. Additionally, empirical parameters such as atomic size difference, mixing enthalpy, and valency electron concentration (VEC) can be used to assess the phase stability [92,93]. Additionally, Floriano et al. [75] considered the use of the enthalpy parameter to optimize the HEAs. The aim was to improve the hydrogen storage capacity and efficiency of alloy materials.

Consequently, an extensive investigation was performed using a density functional theory to predict the enthalpies and identify the most promising material. At high hydrogen concentrations, the interaction between hydrogen and the crystal lattice dominates, affecting the crystal nucleation into new phases. At equilibrium, the chemical potential in the HEAs composition is uniform in all crystal phases, resulting in the system minimum free energy [94,95]. Table 4 presents the value of the thermodynamic parameter for HEAs. Since the phase structure of HEAs has a significant impact on hydrogen storage and application, having an understanding of this structure will be helpful in alloy design.

Table 4. The parameters, VEC, δ, Ω, ΔSmix, and ΔHmix, for typical HEAs reported.

Alloys	VEC	δ	Ω	ΔH_m (KJ/mol^{-1})	ΔS (J/mol^{-1})	Author
AlTiVYZr	3.30	10.95	1.62	−14.88	13.38	[95]
AlCoCrCuFeMoNiTiVZr	6.6	8.54	1.84	−17.24	19.14	[96]
TiZrNbVZn	6.6	6.5	4.62	−31.4	13.38	[97]
ZrTiVCrFeNi	6.17	10.02	1.66	−19.33	14.9	[98]
$V_{35}Ti_{30}Cr_{25}Fe_{10}$	5.25	5.3	2.83	−7.02	10.85	[99]
$V_{30}Ti_{30}Cr_{25}Fe_{10}Nb_5$	5.25	5.7	2.95	−7.48	12.04	[99]
$V_{35}Ti_{30}Cr_{25}Mn_{10}$	5.14	5.0	4.16	−4.55	10.85	[99]
$V_{35}Ti_{30}Cr_{25}Fe_5Mn_5$	5.20	5.2	3.31	−6.04	11.43	[99]
$Co_{32.9}Fe_{34.0}Ni_{33.1}$	9.00	0.40	11.98	−1.35	9.15	[100]
$Cr_{37.0}Fe_{28.9}Ni_{34.1}$	7.94	0.26	3.64	−4.75	9.10	[101]
$Co_{25.3}Cr_{25.5}Fe_{25.3}Ni_{23.8}$	8.22	0.35	5.76	−3.72	11.53	[100]
$Cu_{23.2}Co_{26.5}Fe_{24.9}Ni_{25.4}$	9.47	1.11	4.15	4.65	11.53	[100]
$Al_{28.5}Cr_{27.3}Fe_{24.9}Ni_{19.3}$	6.4	6.49	1.40	13.21	11.46	[102]

2.3.2 Effect of particle distribution and alloying element in HEAs

Particle size and alloying elements can significantly affect the hydrogenation properties of materials. By reducing the particle size through milling, the intermetallic phase disappears, and a more homogeneous solid solution is created, leading to improved hydrogen storage capacity. Additionally, the increased dislocation density and surface area resulting from the milling process can enhance HEA hydrogenation. This process is promising for the development of more efficient hydrogen storage materials [103]. Nonetheless, surface oxidation poses a significant challenge when milling HEA powders due to the increased surface area exposed to oxygen, potentially leading to oxidation. In materials containing elements like Fe, oxidation can result in the formation of oxides such as Fe_2O_3. Therefore, maintaining strict control over the milling atmosphere is imperative to mitigate this issue. Extended milling durations and elevated milling speeds amplify energy input, further exacerbating the problem by promoting greater surface area [104]. Additionally, lattice distortion, as noted in the provided context, can enhance hydrogen solubility by creating interstitial sites with favorable energy levels, which may influence the oxidation behavior during milling.

Milling processes can significantly impact the reproducibility of material properties due to several interacting factors: Parameter sensitivity, viability, and equipment variation. Inconsistencies in the raw materials can lead to variation in the final product, thereby making it difficult to achieve reproducible material properties; however, pre-processing of raw material to ensure uniformity can help in mitigating these issues [105].

Milling costs vary significantly depending on the particle size reduction techniques employed. Different milling methods have varying energy consumption, equipment costs, and operational requirements, which may impact the overall cost of production [106].

HEAs often comprise a blend of chemical elements, notably transitional metals, alkaline metals, and earth alkaline metals. Notable examples include vanadium, nickel, titanium, yttrium, and niobium, which have a strong affinity with hydrogen gas. Vanadium (V) has been studied extensively as a potential material for energy storage due to its high solubility and diffusivity of hydrogen at certain temperatures and pressures. Vanadium (V) is indeed recognized as a strong hydride former that

contributes to increasing hydrogen absorption capacity; in this case, it provides favorable lattice sites for hydrogen occupation. It also enhances hydrogen diffusion kinetics by creating lattice distortions that facilitate hydrogen mobility [107]. The addition of vanadium to TiZrVNiCrFe HEA has been reported to increase the hardness and wear resistance of the alloy, making it potentially useful for a variety of applications in industry and engineering (Table 5) [108].

Table 5. The role of alloying elements.

V and Nb	Nickel	Yttrium
Primarily stabilize phases and provide hydrogen accommodation sites.	Act as a catalyst, thereby improving reaction kinetics and activation, essentially for practical rapid hydrogen charging.	Stabilized hydride thermodynamically and modified lattice characteristics favorably for hydrogen storage

Nickel (Ni) can adsorb and dissociate hydrogen molecules, making it an attractive element for hydrogen storage applications. Nickel (Ni) typically improves activation kinetics by lowering the energy barrier for the initial hydrogen uptake. Additionally, it stabilized hydride phases, favoring reversible absorption and desorption at near-ambient conditions [109]. When combined with titanium to form Ti-Ni alloys, the resulting material exhibits enhanced kinetics for the reaction with hydrogen, making it a promising material for onboard vehicle hydrogen storage. The addition of nickel to titanium also has a significant effect on the properties of the hydrogen storage device. The lattice parameter is reduced when nickel is added. This reduction can lead to a higher concentration of hydrogen atoms in the material. Besides, activation cycles also improved even at room temperature and atmospheric pressure. This improvement increased the efficiency of kinetic hydrogen desorption, which is vital for onboard applications where quick refueling times are necessary [110,111].

The addition of zirconium can also reduce the plateau pressure in a fast-kinetic reaction. The metal will absorb hydrogen more rapidly, enabling the expansion of hydrogen solubility in the solid solution. This effect is specifically exhibited in the high content of zirconium in the alpha phase, thus enabling rapid and massive hydrogen absorption at low pressure [112].

Yttrium is often used as an alloying element in refractory alloys due to its ability to improve phase stability and reduce grain growth at high temperatures [113]. Yttrium usually influences the lattice constant and creates microstructural features influencing hydrogen diffusion pathways. It can also influence the Nano sizing and Nano confinement of the alloy. This is because the small size of the yttrium atoms can create small, confined spaces in the alloy that are ideal for hydrogen storage [114,115].

Similarly, niobium can enhance the performance of hydrogen storage by promoting charge transfer. This weakens the stability of metal hydrides and increases their capacity to store hydrogen. Niobium is a hydride former and improves hydrogen solubility by expanding the lattice structure and providing interstitial sites and also contributes to improving cycle stability; in this case, the phase segregation is reduced during hydrogen uptake and release [116].

To determine the enthalpy and entropy values using the thermodynamic parameters, the equation of Van't Hoff can be explored, as shown in Eq (19) [117].

$$\ln\left(\frac{P_p}{P^o}\right) = \left(\frac{\Delta H}{RT} - \frac{\Delta S}{R}\right), \tag{19}$$

where Pp and Po are expressed as plateau pressure and standard pressure at atmospheric pressure,

respectively. HEAs shows a range of ΔH values typically between −20 to −60 kJ/mol H_2 depending on composition and phase. The lower magnitude of ΔH favor reversible hydrogen storage at near ambient temperature by balancing hydrogen binding strength. ΔS corresponding to disorder changes in the system [118]. In hydrogen storage, ΔS mainly arises from gas phase hydrogen entropy loss when absorbed into the solid. Alloys with optimized ΔH and ΔS enable hydrogen absorption at moderate pressure and desorption near room temperature, thereby maximizing usable hydrogen capacity and energy efficiency [119]. Whenever ΔH is too negative (strong binding), high temperature or vacuum is required for desorption, thereby reducing reversibility and efficiency, and if ΔH is too positive (weak binding), hydrogen would not be stored effectively at practical pressures. If ΔS shift equilibrium curves and affects hysteresis behavior, thus, influencing cycling stability. For instance, TiVNbCrMo HEAs show ΔH around −35 to −40 kJ/mol H_2 enabling reversible hydrogen storage near room temperature with good cycling [120]. In summary, the variation and tuning of ΔH and ΔS in HEAs are fundamental to controlling hydrogen absorption and desorption equilibria via the Van't Hoff equation. These parameters determine practical operating pressure, temperature, reversibility, and energy efficiency crucial for advancing HEAs as hydrogen storage materials [121].

2.4. Potential applications of high entropy alloys for hydrogen storage

HEAs offer several advantages for hydrogen storage, such as tunable properties and enhanced hydrogen uptake capabilities. HEAs can be used in the construction of high-capacity hydrogen storage. This is due to its unique atomic arrangement and high entropy properties, which can enhance hydrogen sorption. It also enables the storage of a large quantity of hydrogen within a given volume and weight of materials [122]. Because of the superior mechanical properties of HEAs, they can be used as structural materials to build a high-pressure hydrogen storage vessel, as illustrated in Table 6 [123]. The nature of these HEAs materials can facilitate rapid hydrogen absorption and desorption where quick refueling or release of hydrogen is required, such as hydrogen fuel cell vehicles and the production of high-purity in industrial processes [94]. Using hydrogen adsorption to cool or refrigerate, HEAs can be used as a promising material for refrigeration systems. This is due to the exothermic nature of hydrogen adsorption processes [124]. HEAs are applicable in the production of portable hydrogen storage devices, such as hydrogen-powered laptops, mobile phones, and other electronic applications for hydrogen storage gadgets, since this material can provide a compact and energy-dense solution for mobile applications [125].

Table 6. The application of hydrogen storage.

H_2 storage applications		
Space exploration	Compression vessel	Portable device -laptop and mobile phone
Fuel cell vehicle	Backup-system	Purification -industrial process
Adsorption refrigeration	Submarine fuel cell	Fuel tank

Solid hydrogen energy storage could be beneficial for submarines, especially in propulsion systems where space is limited and a high energy density is required [126]. In space exploration, where each gram of payload is crucial, HEAs as lightweight materials can be used in the construction of high-capacity hydrogen storage tank for spacecraft and rovers, enabling long missions and improved energy efficiency (Figure 7) [127]. Finally, HEAs can be incorporated in the design and construction

of a backup power system for solar cells and wind energy, especially in critical infrastructure such as hospitals and data centers [128]. Though HEAs possess exceptional promising properties for hydrogen storage across diverse applications, the current limitation has restricted their immediate implementation and application.

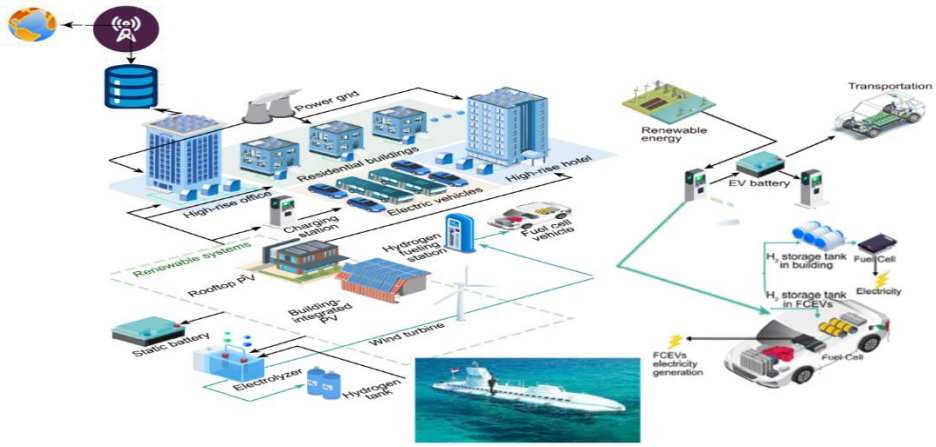

Figure 7. Hydrogen energy hubs for district resilience [129].

2.5. Prospect and limitation of HEAs for hydrogen storage

Industrializing HEAs for hydrogen storage hinges on minimizing materials and energy costs (Table 7) while addressing production scale challenges, alongside exploiting their intrinsic high-performance benefits. This integrated perspective will guide research and development toward economically viable large scale HEA hydrogen storage production [130–132].

Table 7. Current limitation of HEAs for hydrogen storage.

Material cost	Synthesis energy consumption	Large scale production	Industrialization perspective
Cost competitiveness of raw materials such as precious stone, costly transition metals—Nb, Ti, Hf, V, and Zr. This raw material is expensive when compared with traditional hydrogen storage materials, thus impacting the overall economic feasibility. Solution: strategies of reducing the cost by using recycled elements and developing secondary synthesis routes using scrap material.	Production of HEAs often requires energy intensive. The energy cost for synthesis influences the carbon footprint and commercial scalability of HEAs hydrogen storage application.	Process control for repeatability and defect minimization is essential to ensure consistent hydrogen storage performance on industrial scales.	The cost of metal printing, affected by product volume and complexity, will enable an evaluation of conditions where advanced manufacturing techniques are favored over conventional techniques. Realizing the practical hydrogen storage solution using HEAs requires balancing superior material properties with cost-effective, scalable manufacturing.

3. The design of HEA alloys, synthesis, and potential applications

The HEAs potential for energy storage is discussed considering the alloys thermal properties and their kinetic reactions. Many HEAs exhibit remarkable thermodynamic stability at high temperatures, making them suitable for energy storage [133]. Furthermore, the solubility of hydrogen in HEAs varies depending on the alloy compositions and the conditions under which it is used [134].

Understanding the factors and their interactions is vital for developing HEA-based materials with optimal properties for hydrogen storage [135]. In the context of hydrogen absorption or desorption, a higher value of heat of formation (ΔH) would be required for more heat to be released or absorbed during the kinetic reaction process. Hence, the heat of formation (ΔH) is paramount in determining the stability of hydrogen in the HEAs. High-entropy alloys usually exhibit high volumetric density and low-pressure storage features, and this is due to the formation of a disordered solid solution and their low density in gaseous form, which makes them difficult to store in large quantities. Moreover, its poor mass and heat transfer are also a setback. When hydrogen diffuses into metal hydrides (HEAs) or intermetallic, it forms a solid solution with an α-phase. As the hydrogen pressure and concentration increase, the host metal or alloys (HEAs or metal hydrides) begin to form an β-phase [136]. This phenomenon translates into a thermodynamic process known as pressure composition isothermal (PCI). Whenever equilibrium is reached, the two phases coexist, showing plateaus in the PCT curves. At this point, the heat dissipation and absorption processes were under control, enabling the storage system to operate at equilibrium pressure (Peq) and constant temperature, as expressed in Eq (20) [137].

$$\text{HEAs} + \frac{X}{2}H_2 \longleftrightarrow \text{HEAs } H_x + \text{Heat},$$

$$P_{eq} = \exp - [\frac{\Delta H}{RxT} - \frac{\Delta S}{RxT}], \tag{20}$$

where Peq denotes the pressure equilibrium.

Specific assumptions are made about the mechanism of energy transfer using a set of equations in the development of the model. These assumptions are:

[a] Hydrogen gas phase obeys the perfect gas law and behaves as a thermodynamic ideal gas;

[b] Solid phases are isotropic with a uniform porosity distribution;

[c] Medium has a characteristic of local thermal distribution;

[d] Thermophysical properties are constant;

[e] Heat convection and radiation are negligible in the metal hydride, while the mode of heat transfer in the media phase is conduction; advection transport is negligible, and the HEAs-phase composition system is adiabatic.

Heat removal is essential for maintaining the continuity of a kinetic reaction and for cooling the bed of a HEA. The mechanism for heat removal may involve the use of a coolant or a cooling system, which can either be internal or external to the HEA. Regarding the governing equations of hydrogen flow, it is necessary to make certain simplifying assumptions to enable mathematical modeling and analysis. Nonetheless, it is important to note that in some situations, the assumptions in [a–e] may not hold, and more complex models and equations might be required to accurately describe the behavior of the system. Hence, for the application of any modeling or analysis to a specific problem, it is necessary to carefully evaluate its assumptions and limitations [138,139].

The expression of heat transfer associated with the reaction of the hydrogenated HEAs or metal hydride bed are given in Eqs (21–23). This is the governing equation for energy transferred by conduction.

$$\rho C_p \delta T \frac{\delta T}{\delta t} + \rho_g Cp_{g(}((U.\nabla T) = \nabla x(K_e \nabla T) + Q_{s,} \quad (21)$$

$$(\rho Cp)_e = \varepsilon^* \rho^* C_{pg} + (1 - \varepsilon)^* \rho_{m^*} Cp_{m,} \quad (22)$$

$$\lambda_{e\,=} \varepsilon^* \lambda_g + (1 - \varepsilon)^* \lambda m, \quad (23)$$

where $C_{p,}$ represents specific heat capacity, ρ indicates density of the fluid or gas, u is the velocity, T and Q stand for heat sinks and temperature, while Ɛ and K were expressed as porosity and thermal conductivity, respectively. The subscripts e, g, p, m, and s represent effective gas pressure, metal, and sink, respectively.

The heat and mass transfer processes for HEA must be thoroughly investigated, as well as the technology involved in the physical phenomenon, storage design, and geometry.

3.1. Mass balance equation

Mass balance equations are essential in the design and optimization of hydrogen storage systems. It is a potential tool for assessing the size of storage tanks and flow rates [140]. Using this equation, one can evaluate the system efficiency and emissions, which are quite critical for the sustainability of hydrogen energy storage. The mass balance equation always ensures that the principle of conservation of mass in the system is upheld, which is indispensable in chemical reactions and metal flow. Hence, mass conservation laws state that the total mass of a closed system remains constant over time [141]. In the case of hydrogen gas flow, especially in a metal bed, the mass of hydrogen entering must be equal to the mass of hydrogen leaving the metal bed, thus obeying the fundamental principle of mass conservation. Hydrogen is rather absorbed and desorbed in a reacting metal bed, thus causing changes in the solid density. The mass flow rate $\dot{m}$ is defined as the mass of hydrogen absorbed and desorbed per unit of time and volume, as buttressed in Eq (24) [142].

$$\dot{m} = \rho A \nu, \quad (24)$$

where $\dot{m}$ represents the mass flow rate, ρ indicates the density, and A and ν denote the surface area of the porous metal bed and hydrogen flow rate, respectively.

Nevertheless, if the solid material remains incompressible, any changes in solid density can be ignored. Thus, the mass flow rate of hydrogen is usually dependent on the hydrogen flow rate and the surface area of the metal bed. This relationship is based on the assumption that hydrogen flow is uniform and that there are no significant changes in pressure or temperature along the length of the metal bed. Eqs (25–27) obey the law of perfect gas [143].

$$\dot{m} = (1 - \varepsilon) \frac{\delta \rho s}{\delta t}\ , \quad (25)$$

where Ɛ, dps, and dt denote pressure with respect to time and emissivity of hydrogen bed.

Here, the hydrogen gas behaves as an ideal thermodynamic gas and thereby obeys the law of perfect gas.

$$\dot{m} = \varepsilon \delta \rho_g + \frac{1}{r} \frac{\delta}{\delta r} (r \rho_g u_r) + \frac{\delta}{\delta z} (\rho_g u_z), \quad (26)$$

where r and z are radially and longitudinally coordinated, respectively.

Additionally, ρ_g, as expressed in Eq (19), is given as

$$\rho_g = \frac{MgPg}{RTg}, \tag{27}$$

3.2. Kinetic reactions

The absorption and desorption of hydrogen gas in any material often involve kinetic reactions, which may be closely affected by environmental conditions such as temperature, pressure, and material properties. There are many sequences of steps involved in a kinetic reaction, and this includes the transition of adsorption to the absorption state, bulk diffusion, dissociative chemisorption, mass transport of hydrogen gas, and surface migration. A high temperature and low pressure will favor desorption, while a lower temperature and high pressure will influence absorption. When a HEA is heated, the hydrogen is released through thermal desorption. The dissociation of hydrogen molecules into atomic hydrogen, followed by the diffusion of hydrogen into the metal lattice, increases the absorption influence. These processes are illustrated in Eqs (28,29).

For the absorption case:

$$\dot{m} = C_a \exp\left(-\frac{Ea}{RT}\right) \ln\left(\frac{Pg}{Peq}\right) [\rho_{sat} - \rho_s] \tag{28}$$

For the adsorption case:

$$\frac{\delta\rho s}{\delta t} = C_a \exp\left(-\frac{Ea}{RT}\right) \ln\left(\frac{Pg}{Peq}\right) [\rho_{ss} - \rho_s], \tag{29}$$

where Ca denotes the material-dependent constant, Ea is given as activation energy, ρss is expressed as density of the solid phase at saturation, ρs, indicates the density of the solid, Pg, and Peq represent gas pressure, and equilibrium pressure respectively, while $\frac{\delta\rho s}{\delta t}$ is given as the pressure gradient.

$$\ln\frac{P_p}{P^0} = \left(\frac{\Delta H}{RgT} - \frac{\Delta S}{Rg}\right),$$

and then rewritten as

$$\ln P_{eq} = \left(\frac{\Delta H}{RgT} - \frac{\Delta S}{Rg}\right),$$

Heat transfer can significantly impact the rate at which absorption or desorption occurs and the overall efficiency of the process. The process of heat transfer by conduction is responsible for transferring thermal energy between substances that are in direct contact and is expressed as Eq (30):

$$\frac{q_x}{A} \sim \frac{\delta T}{\delta x} \tag{30}$$

where $\frac{\delta T}{\delta x}$ is denote as the temperature gradient in the direction of heat flow; q_x is the thermal conductivity of a material with surface area A.

From Eq (31), the thermal conductivity q_x, which is the rate of heat transfer per unit area, is proportional to the normal temperature gradient and is given as

$$q_x = -kA\frac{\delta T}{\delta x}, \tag{31}$$

Additionally, in a steady-state system, a one-dimensional system where heat flows in a cylindrical coordinate (especially in the absence of heat generated in the cylinder), the energy flow rate is given as Eq (32) [139]

$$\frac{d^2T}{dr^2} + \frac{dT}{rdr} = 0 \tag{32}$$

3.3. Thermal conductivity of hydrogen gas

In the case of hydrogen gas, thermal conductivity usually occurs through the mechanism of molecular collision. When gas molecules collide with each other or with the walls of the container, thermal conductivity arises through lattice vibrations and electron transport [144]. The numerical value of thermal conductivity for any material depends on many factors: The specific heat capacity of the material, density, molecular or atomic structure, temperature, and pressure. Since hydrogen is a diatomic gas, its thermal conductivity usually increases with temperature. In general, materials with high thermal conductivity tend to have a high density or high molecular weight and a crystal structure that allows for efficient heat transfer [145].

The absolute dependence of this density has a significant effect on thermal conductivity, meaning that an increase in gas density will result in a reduction in thermal conductivity, especially at lower pressures. Moreover, as the pressure increases, hydrogen gas tends to behave as an ideal gas, and the relationship becomes more complex. Nonetheless, the presence of impurities will cause the thermal conductivity to deviate from the ideal gas behavior [146].

3.4. Phase change materials

The energy equation for a phase-change material (PCM) is based on the enthalpy formula. In this case, the equation will be expressed in terms of temperature and total volumetric enthalpy. As a result, the thermal and physical properties will be determined. It includes both internal and external energy, which are required to overcome any external forces, such as pressure or volume changes [142]. When a PCM undergoes a phase change, either from solid to liquid or liquid to gas, it absorbs or releases a large amount of latent heat, which is not reflected in temperature measurements [143]. Modeling PCMs is not always easy due to their complex behavior. For instance, PCM sometimes undergoes a partial phase transition in a real-life operation. As such, the energy equation needs to be modified to include the effects of latent heat. This will enable more accurate predictions of the temperature distribution and energy transfer within a PCM system.

In the context of a phase change, the chemical potential reflects the equilibrium conditions between two phases. A binary alloy of metal and hydrogen requires equal chemical potential between the two coexisting phases to reach thermodynamic equilibrium [147]. As such, the mass transfer between phases will be under control, thus influencing the stability and boundary phase of alloys [148]. The plateau pressure is observed when the system reaches a state of dynamic equilibrium. At this point, the rates of hydrating and dehydrating become equal, and there are no net changes in the amount of hydrogen in the metal lattice.

The occurrence of a plateau-pressure in HEAs-hydride systems is due to the limited diffusion rate of hydrogen in the metal lattice. When the alloy is heated, hydrogen desorbs from the metal lattice, creating a high-pressure region close to the metal surface. This high-pressure region will lead to a plateau in pressure as the pressure increases and the hydrogen diffusion reduces, as expressed in Eqs (33,34) [149].

$$\frac{\delta H}{\delta t} = \nabla.\,[(\lambda_{pcm}\nabla(T))], \tag{33}$$

$$\text{But } H(T) = h(T) + \rho_{pcm}\, L f\,(T),$$

where L is the latent heat of the phase of the composition material, $f(T)$ is the liquid fraction, and H(T) is the total enthalpy, which is defined as the sum of the sensible enthalpy h(T), given as h(T).

$$h(T) = \int_{T_m}^{T} \rho pcm\; C_p pcm\; dT, \tag{34}$$

where ρpcm, $C_p$cm, and lpcm are given as the density, specific heat, and thermal conductivity of the PCM, respectively.

In Figure 8, PCM demonstrates a number of properties during heat exchange, including: [a] Low volume expansivity during the phase change; [b] high latent heat of fusion for thermal energy during the exothermic and endothermic reactions; and [c] sufficient melting temperature, but higher than ambient temperature and lower than the maximum-minimum temperature that occurred during the sorption reaction process [150]. Finally, PCM must be thermally stable over a large number of thermal cycles and also maintain the phase change transition and structural properties.

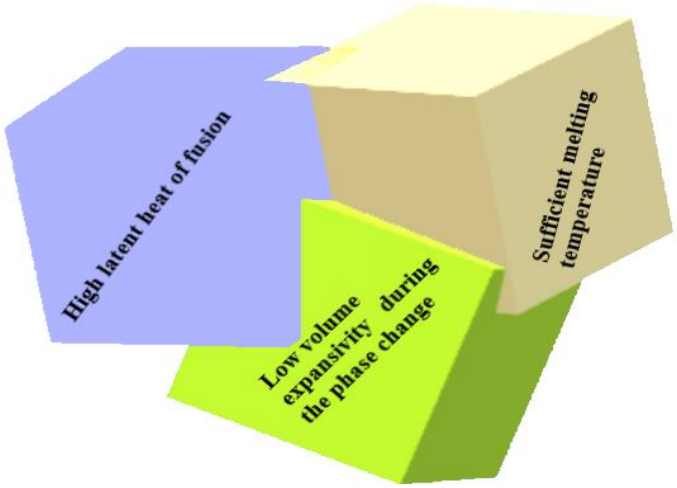

Figure 8. The characteristics of phase-change materials.

The integration of PCMs into HEAs for thermal management in hydrogen storage is critical. PCMs, by absorbing and releasing latent heat during phase transitions, stabilize temperature fluctuations during hydrogen absorption and desorption cycles in HEA storage beds [151]. Incorporating a heat exchanger with PCM units in thermal contact with HEA beds enables controlled heat supply and removal. In this case, it ensures a stable temperature and prevents hot spots and thermal gradients that can adversely affect hydrogen absorption and desorption [152]. PCMs act as buffers

surrounding or embedded within HEA beds, improving cycling efficiency and durability. For example, researchers have explored Ti-Zr-Hf-Ni-Cu HEAs and their phase transition behavior as solid-solid PCMs for high-temperature thermal energy storage [153].

3.5. Momentum equation for hydrogen flow

The momentum equation of a hydrogen flow gas is a fundamental equation in fluid dynamics that describes how the velocity of the liquid changes with time due to forces and gradients (pressure, viscosity, and gravity) [154]. This equation can be used to analyze and predict fluid flow behavior. Under a boundary and initial condition, the specific behavior of hydrogen gas can be modelled [155]. Figure 9, illustrates hydrogen gas flow in a storage component. As the gas travels through the HEA bed, it will undergo various mechanisms: Surface diffusion, lattice diffusion, and grain boundary diffusion. The dominance of a particular diffusion mechanism depends on many factors, such as temperature, pressure, and the microstructure of the HEAs. For instance, at a lower temperature, lattice diffusion may be more dominant, while at a higher temperature, surface diffusion or grain boundary diffusion might play a significant role [156,157].

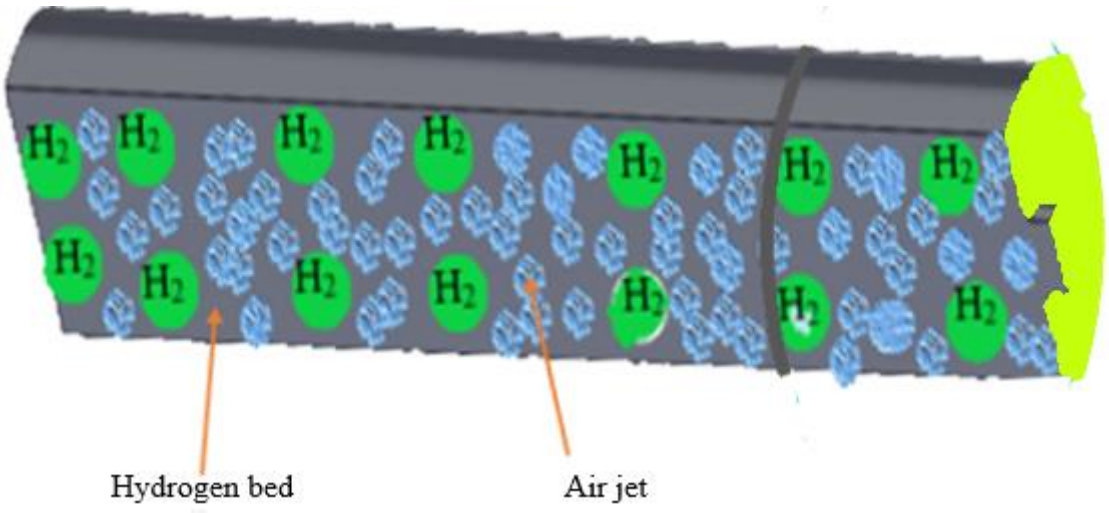

Figure 9. Geometry of hydrogen energy storage component.

$$\rho\frac{\delta P_p}{\delta t} = -\frac{\delta P_p}{\delta r} + \mu\left[\frac{\delta}{\delta r}\left(\frac{1}{r}\frac{\delta}{\delta r}(ru_r)\right) + \frac{\delta^2 u_r}{\delta z^2}\right] - \rho\left(u_r\frac{\delta u_r}{\delta r} + u_z\frac{\delta u_r}{\delta z}\right) - S_r, \tag{35}$$

$$\rho\frac{\delta u_z}{\delta t} = -\frac{\delta P_p}{\delta z} + \mu\left[\frac{\delta}{\delta r}\left(\frac{1}{r}\frac{\delta}{\delta r}(ru_z)\right) + \frac{\delta^2 u_z}{\delta z^2}\right] - \rho\left(u_r\frac{\delta u_z}{\delta r} + u_z\frac{\delta u_z}{\delta z}\right) - S_z, \tag{36}$$

P_p hydrogen pressure, where S_r and S_z are the pressure drops of the hydrogen gas due to viscous dissipation as buttress in Eq (35).

$$S_i = \left(\frac{\mu}{K}\right)u_i, \tag{37}$$

where μ (kg/ms) indicates the dynamic viscosity of the hydrogen gas and K (m^2) represents the thermal permeability of the porous bed.

The mass and momentum balance Eqs (24–37) used for hydrogen storage systems with HEAs often rely on assumptions that simplify the real-world behavior of these materials. Such assumptions include quasi-steady-state flow or steady-state flow, ideal gas behavior of hydrogen, isotropic porous media properties, and simplified geometrics or thermal boundary conditions [158,159]. These models provide a theoretical framework, and their validation with actual HEA materials is lacking, with studies often focusing on analogous metal hydride systems [160]. Researchers need to focus on integrated experimental-modelling approaches to explicitly test these equations under practical HEA bed conditions, especially considering transient behavior during charging and discharging cycles. Validation should include measurements of hydrogen uptake, pressure profiles, temperature changes, and dynamic flow through porous HEA compacts, comparing these measurements with model predictions [161]. Furthermore, models need to incorporate evolving microstructure changes, phase transitions, and hysteresis to more accurately reflect the dynamics of hydrogen storage in HEAs, as lattice distortion can enhance hydrogen solubility by creating interstitial sites with favorable energy levels [162].

3.6. Thermal diffusivity

In solids, liquids, or gases, thermal diffusivity and thermal conductivity play very different roles depending on whether the heat supply is steady-state or transient. In a steady-state measurement of heat transport, only thermal conductivity takes precedence while the diffusivity has a partial effect [163,164]. However, if the heat supply varies as a function of time, then the diffusivity determines how the temperature ranges within a material in response to a thermal gradient [165]. The choice of alloy composition in HEAs also has an impact on thermal diffusivity. Since each of these alloys has varying thermal properties, their combination in HEAs may influence heat conduction [35]. Similarly, in hydrogen interaction, the presence of hydrogen gas in the HEAs can affect the thermal diffusivity and consequently alter the heat transfer. Moreover, hydrogen absorption into HEAs is often exothermic. The energy released in the form of heat will cause a rise in temperature within the HEAs [166]. Hence, adequate control of temperature is required to avoid undesirable effects such as excessive desorption and reaching temperature limits. The thermal diffusivity (α) of a material is expressed in Eq (38) [167].

$$\frac{1}{\alpha}\frac{\delta T}{\tau} = \frac{\delta^2 T}{\delta x^2} + \frac{\delta^2 T}{\delta y^2} + \frac{\delta^2 T}{\delta z^2} + \frac{\dot{r}}{k}, \tag{38}$$

where $\alpha = \frac{K}{\rho C_p}$, with density(ρ) d(T), and thermal conductivity (K) while x, y, and z are variables with respect to temperature.

A higher value of thermal diffusivity α signifies a faster rate of heat transfer, which is often associated with a lower specific heat capacity (Cp). This means that materials with high thermal diffusivity tend to absorb less heat to increase their temperature, allowing them to respond more rapidly to thermal changes. Consequently, when the heat capacity is lower, the material requires less energy to achieve a given temperature rise, enhancing its efficiency in thermal applications.

Effective heat management in practical HEA hydrogen storage systems is critical due to the

exothermic and endothermic nature of hydrogen absorption and desorption [168]. HEAs possess variable thermal conductivities, tailored by composition and microstructures to balance mechanical stability and thermal properties [169]. Heat exchangers integrated with HEA beds manage heat during cycling, while embedding high thermal conductivity additives within HEA powder beds enhances internal heat transfer [170]. Optimizing particle or pellet size and packing density of HEAs maximizes surface area for heat exchange while maintaining hydrogen permeability. The use of phase change materials (PCM) surrounding HEA beds stabilizes temperature by absorbing heat spikes during absorption and desorption process. Alloy compositions are carefully chosen for thermal properties, external and internal heat transfer enhancements are integrated, and reactor design is optimized to ensure stable, efficient hydrogen absorption and desorption cycling. Lattice distortion can enhance hydrogen solubility by creating interstitial sites with favorable energy levels [171].

Integrating system-level performance simulation into the design process enables a thorough understanding of practical engineering for hydrogen storage. Simulations based on HEA material properties can help in maximizing hydrogen absorption and desorption efficiency in reactors and storage tanks [172]. The mechanism of modelling of this heat exchanger and reactor will help in integrating hydrogen storage units to ensure effective thermal management during exothermic and endothermic reactions. According to Sahlberg et al. [173] TiVZrNbHf alloys absorbed hydrogen above 200 °C due to a reduction in hydrogen pressure in the reactor, but a complete hydrogenation at 400 °C for 48 hours produced a BCT lattice. Furthermore, when the hydrogen storage system cycle is simulated, the kinetics, thermodynamics, heat flow, and pressure changes can be evaluated [173]. Studies have shown that increasing the surface area of the heat exchanger can improve hydrogen absorption and desorption. HEAs, intrinsic lattice distortion and complex elemental interactions may contribute to exceptional hydrogen capacity and reversible storage. Nonetheless, system performance hinges on stability under cyclic hydrogen charging, resistance to embrittlement, and mechanical integrity at operational temperature and pressure [174]. During this, considerable system parameters, such as HEAs, thermal conductivity, and strain tolerance, will be required because they will influence the storage cycle time and structural longevity.

The pronounced low thermal conductivity of HEAs is demonstrated through the basic experiment. This experiment involves comparing HEAs with several reference samples to highlight the difference in thermal conductivity. The total thermal conductivity (κ), electron thermal conductivity (κe), and phonon thermal conductivity (κl) of $(CoNi)_{50}(TiZrHf)_{50}$ compared with a variety of FCC alloys (Table 8).

Table 8. Thermal conductivities of HEAs [175].

	κ	κ_e	κ_l
Alloy	(W/(mÂ·K))	(W/(mÂ·K))	(W/(mÂ·K))
Ni	88	88	0
CoNi	68.4	58.9	9.5
CoCrNi	11.4	7.2	4.2
AlCrFeNi	16.7	11.3	5.4
FeCoNiCr	12.8	8	4.8
FeCoNiCrMn	13.7	6.8	6.9
FeCoNiCrPd	10.3	4.8	5.5
$(CoNi)_{50}(TiZrHf)_{50}$	8.4	7.8	0.6

3.7. The interactions of the hydrogen ion with HEAs

The interaction of the hydrogen proton ion with HEAs occurs through several processes. Among these is the diffusion process, where the proton diffuses through the lattice structure of the alloy [35]. The interaction between the proton and the alloy can also involve other processes, such as adsorption and desorption. Hydrogen bonding occurs at a wide range of energy levels. If the overlapping is positive, bonding interactions would occur in the atoms [176]. Since hydrogen occupies the interstitial sites, as earlier mentioned, it can delocalize under any stress condition. Thus, any alloy that resists stress will typically alter the hydrogen solubility [122]. This could have a significant impact on the lattice parameter and the hydrogen concentration at the initial α-phase. When the concentration of hydrogen exceeds the terminal solid solubility, a second β-phase (VH/V_2H) will form. The final γ-phase (VH_2) precipitated more as the concentration increased.

3.7.1. Crystal Orbital Hamilton Population (COHP)

As hydrogen reacts with HEAs, a chemical bond forms between hydrogen and the metal atom. These chemical bonds usually vary depending on the specific element involved, such as a metallic bond [177]. The strength of the chemical bond will be evaluated using COHP. This will help in determining the hydrogen-induced effect on the electronic structure of the alloys [178]. Besides, the hydrogen-induced effect can introduce energy levels within the band gap, affecting the electronic transition [179,180] as it influences the material's appearance and reflectance. As a function of temperature and pressure, hydrogen solubility varies in HEAs [181,182]. Changes in solubility can impact the extent of the hydrogen-induced effect on electronic and optical properties [183].

COHP has been demonstrated to be an excellent tool for identifying the various hydrogen-HEA interactions [184]. However, its analysis only relies on the symmetry of the crystal lattice; therefore, it is equally important to ensure that symmetry considerations are appropriately addressed to obtain an accurate result [179,185].

3.7.2. Electron Localization Function (ELF)

The electron distribution will be determined through the electron localization function, which will reveal the nature of the chemical bond and the location of the electron pair. In a region where a high concentration of electron pairs is found, hydrogen ions will interact with metals in HEAs [129–131]. However, in a location where the bond is critical, the electron density is at its minimum level [132,186]. Hence, the spatial representation of an electron localization will show where the electron density is high or low [187].

The diffusion of hydrogen occurs along the migration path within the HEA lattice. Changes in the external environment can influence the electronic structure and geometry of an alloy, thereby indirectly affecting the value of ELF. For instance, during thermal expansion, temperature changes can alter the interatomic distance within the HEAs, thus, influencing the ELF values [130,134]. Similarly, a high temperature will raise the vibration motion, leading to changes in electron density distribution in the region of high concentrations of atomic bonds [188,189]. Since high temperatures promote electron excitation, this will lead to an alteration in the electron density distribution and could potentially affect the ELF values [190].

Furthermore, a change in pressure will lead to compression or expansion of the HEAs, thus affecting the interatomic distance and overall density and, consequently, influencing the ELF value. High pressure induces changes in the electronic band structure of HEAs, and this affects the electron distribution. In addition, phase transitions may also occur, leading to changes in crystal. Moreover, other factors, such as the chemical composition and temperature of the alloy, and the properties of the proton, will also influence the interaction [191–193].

The combination of COHP and ELF helps in probing the electronics environment of hydride phases, classifying how each element impacts hydrogen absorption sites, migration paths, and interaction strength, which correlate with experimentally observed storage capacity and kinetics [194]. For instance, the hydrogen permeation investigation of AlCrFeTiNb and AlCrMoNbZr HEA coatings utilized electronic structure and phase analyses, which showed that elements like Fe influence hydrogen permeability and trapping [195]. These tools are useful in understanding why some coatings resist hydrogen storage design. To comprehend hydrogen activation and transport, ELF can be used to model the complexity of hydrogenase enzymes [196].

4. Thermodynamics of high entropy alloy-hydrogen systems

The HEA-hydride system is a complex phenomenon that affects the structural performance of the HEAs. As hydrogen is diffused into the HEA, phase transformations occur; in this case, atoms move from a high-concentration region to a lower-concentration region, typically from the surface to the interior of the HEAs. At elevated temperatures, the redistribution of alloying elements at the interface occurs, which can further affect the phase transformation [197]. The chemical potential of each element in an alloy usually depends on the composition and concentration in the various phases, while at equilibrium, they show an identical phase with the minimum free energy [198].

There are three phases observed in the crystalline structure of BCC, including the saturated α-phase, unsaturated phases, and intermediate hydride, with a crystal phase structure of β, respectively. These phases coexist and lie in a state of equilibrium, with their composition varying with temperature and hydrogen pressure [12]. The metals vanadium (V), niobium (Nb), and tantalum (Ta) are examples of alloys that exhibit these behaviors and form solid solutions with each other [199–201]. Similarly, the atomic or molar fraction of each metal alloy in one phase will be the same in other phases, and it can be represented as $\sum Ci = 1$ Eq (39) describes the behavior of either a saturated entropy metal alloy or an unsaturated metal hydride phase, and the chemical potential of each phase is found to be the same at the point of equilibrium.

Figure 10, describes the Gibbs free energy of the α and β phases as a function of the compositional variable C_H. In this case, the two phases are the same, and they both coexist with hydrogen gas only when the C_H of both phases is the same. while the combined metals in HEAs with chemical potential are the same in both phases. Moreover, in a hydrogenated HEAs system in para-equilibrium at a given temperature, the Gibbs free energy of these phases only depends on C_H. Besides, at reasonable cooling rates under ambient conditions, an intermetallic phase (β) tends to form a single phase (α) after solidification.

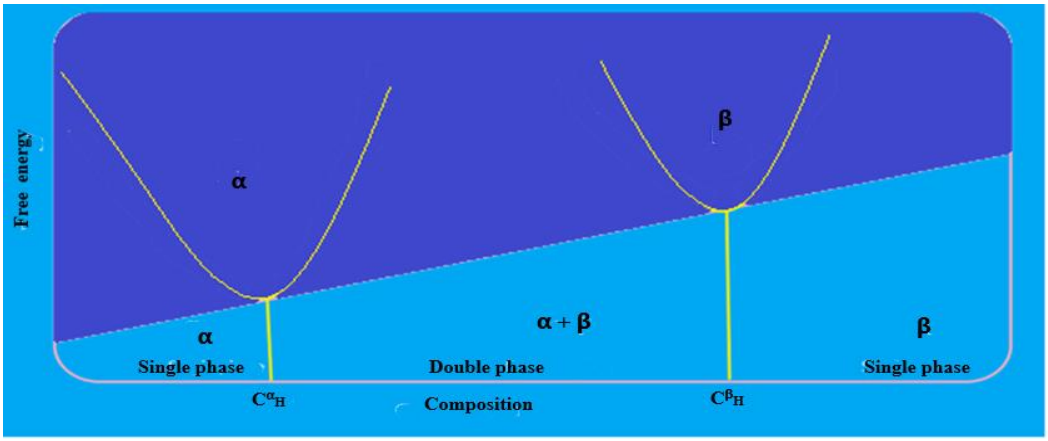

Figure 10. The Gibbs free energy of α and β phase as a function of compositional variable [202].

$$\mu_H{}^{\alpha} = \mu_H{}^{\beta}, \tag{39}$$

where μ_H is the hydrogen chemical potential for α and β phases with compositional variable C_H, given in expression.

$$C_H = \frac{n_H}{n_m}, \tag{40}$$

While at the equilibrium point, where the chemical potentials are equal, the energy required to add or remove atoms will be the same across all phases. This is because the system has reached a state of minimum Gibbs free energy, where there is no driving force for further changes to occur. In this case, the mobility of metal atoms will be restricted at low temperatures, except for the hydrogen atom, which moves without any restraint. Therefore, para-equilibrium arises from the disparity in mobility between rapidly diffusing hydrogen atoms and the slower-moving heavier alloy atoms in HEAs. This concept has significant implications for both hydrogen storage cycle life and storage density [203].

Regarding cycle life, the limited mobility of alloy atoms under para-equilibrium conditions ensures that the alloy's structure remains relatively stable during repeated hydrogen absorption and desorption cycles. This stability mitigates rapid elemental redistribution, phase segregation, cracking, and embrittlement, thereby enhancing cycle life and mechanical durability [204]. Furthermore, the slow redistribution of alloy atoms helps maintain consistent hydrogen sorption sites, stabilizing performance over numerous cycles.

In terms of storage density, para-equilibrium preserves the existing alloy phases during hydrogenation, preventing complete phase transformations that would involve substantial atomic rearrangements. This preservation is crucial for maintaining high storage density by avoiding the formation of undesirable phases that could reduce hydrogen capacity and cause lattice expansion or pore closure [205]. Additionally, lattice distortion, as highlighted earlier, can further enhance hydrogen solubility by creating interstitial sites with favorable energy levels, facilitating rapid hydrogen uptake and reversible storage at designed densities without significant alloy lattice reorganization [206].

Figure 11, describes the pressure-composition-isothermal nature of the hydrogen mixing in the α- and β-phases. At low pressure, only the α-phase coexists in equilibrium with hydrogen gas, and its C_H composition depends on it; however, above the plateau pressure, only the β-phase is in equilibrium

with hydrogen gas. As the composition changes the transitions between these crystal structures and the pressure vary accordingly PH_2 [202].

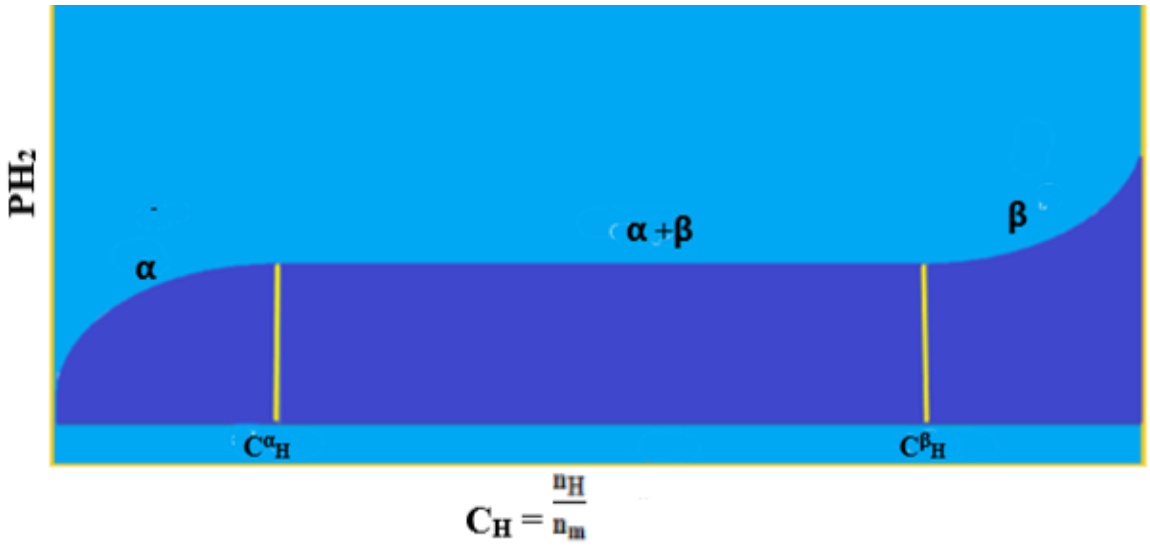

Figure 11. The pressure-composition-isothermal in the α and β-phase [202].

Here, we present a method of system hydrogenation in multiple steps, utilizing the temperature dependence of the isotherms to improve efficiency. The mobility of HEA atoms is limited, but not for hydrogen atoms, and consequently, a new thermodynamic equilibrium, known as para-equilibrium, is introduced to address this limitation in HEA [207,208]. Para-equilibrium considers the difference in mobility between hydrogen and HEA atoms, leading to the formation of two distinct chemicals in hydrogen, and HEA [209]. The chemical potential of an alloy in the α-phase differs from that in the β-phase, except in rare cases where they are similar. Nevertheless, the chemical potential of hydrogen atoms is the same in both α and β phases. The equilibrium phases depend on the changes in Gibbs free energy and the chemical variable of hydrogen content due to the para-equilibrium condition. The Gibbs free energy of hydrogen mixing appears in α and β-phases, as described in Eq (36) [210].

Various methods have been employed to analyze the thermodynamic properties of HEAs in a para-equilibrium condition. One of these approaches is to use the CALPHAD method. This method involves the use of thermodynamic databases and phase diagram software to model the behavior of complex multi-component systems. Another approach is the use of first principles, which entails the use of quantum mechanical calculations to predict the electronic and atomic structures of materials [16,211].

$$\Delta G_m(C_H) = \Delta H_m(C_H) - T\Delta S_m(C_H), \tag{41}$$

where $\Delta G_m(C_H)$ indicates the changes in Gibbs free energy between phases and the enthalpy of mixing (ΔH_m).

As the hydrogen gas is subjected to higher pressure, its solubility in the crystalline phases (α and β) will increase. In this case, the hydrogen will dissolve into the crystal lattice, consequently increasing the size of the crystalline cell [212,213]. Furthermore, whenever the particles in the α and β phases

come into contact with each other, the two atoms present at the boundary interface will experience a change in the enthalpy of mixing (ΔHm). This enthalpy will later be determined using the width of the boundary and the amount of surface area per unit volume [214].

To account for the entropy of mixing within the thermal regime, the entropy equation must include a concentration term. This is because the entropy of mixing is dependent on the concentration of the two substances, which coexist in multiple phases. Despite this, its major challenge is the creation of a liquid miscibility gap in the phase diagram and alloying failure [215]. The concepts of enthalpy and entropy of mixing are very important to understand the behavior of hydrogen gas under different conditions. As a result, the sorption rate and exposure of HEAs to hydrogen will be determined by combining all the models above. As expressed in Eqs (42–43), using "B" as a symbol for representing the HEAs [216].

$$\Delta H_A(C_m) = H^{BH}{}_{CH} - H^{BHalloy} - \frac{c_H}{2} H^{H_2}, \tag{42}$$

$$\Delta S^2(_{CH}) = S^{BH}{}_{CH} - S^{BHalloy} - \frac{c_H}{2} S^{H_2}, \tag{43}$$

where $H^{BHalloy}$ and $S^{BHalloy}$ are the enthalpy and entropy of alloys in the α and β crystal phase structure, C_H denotes composition, H^{BH}, and S^{BH} are the normal enthalpy and normal entropy of hydrogen gas, while H^{H_2} and S^{H_2} indicate the standard enthalpy and entropy of hydrogen respectively.

Some of the HEAs usually form metal hydrides with similar composition but different crystalline structures after they have been hydrogenated, such as BCC-BCT-FCC-hydride. This phenomenon occurs in the thermodynamic para-equilibrium condition of temperature and atmospheric pressure at times, which is the concept of body-centered cubic (BCC) HEA in disordered solid solutions. For instance, TiVZrNbHf alloys, when hydrogenated, form a BCT phase, which is a monohydride stable structure at lower pressure and a dihydride stable structure of FCC at high pressure [76,217].

As stated, Gibbs free energy can establish a thermodynamic condition for phase formation. For the α and β phases with similar chemical compositions, the Gibbs free energy for each phase can be written as a function of C_H, as expressed in Eqs (44–46). Therefore,

$$\Delta G^{\alpha}(_{CH}) = G^{(BH\alpha)}{}_{CH} - G^{alloy} - \frac{c_H}{2} G^{H_2}, \tag{44}$$

$$\Delta G^{\beta}(_{CH}) = G^{(BH\beta)}{}_{CH} - G^{alloy} - \frac{c_H}{2} G^{H_2}, \tag{45}$$

Similarly, any other hydride and intermediate hydride phases emerge as θ with the same composition

$$\Delta G^{\theta}(_{CH}) = G^{(BH\theta)}{}_{CH} - G^{alloy} - \frac{c_H}{2} G^{H_2}, \tag{46}$$

where G^{alloy} is expressed as the Gibbs free energy of alloys in the α, β, and θ crystal phase structures, $\Delta G^{(BH\alpha)}$, $\Delta G^{(BH\beta)}$, and $\Delta G^{(BH\theta)}$ are given as Gibbs free energy of hydrides in α, β, and θ phases with the same chemical composition, respectively. G^{H_2} indicates the standard Gibbs free energy of hydrogen.

Also, the value of these energies, ΔG^{α}(CH), ΔG^{β}(CH), and ΔG^{θ}(CH) largely depends on alloy composition and the crystal structure of high-entropy hydrides. This will provide a significant achievement in the thermodynamic para-equilibrium, especially where the chemical potential of all

components exists side by side in the crystal structure of α, β, and θ, as shown in Eqs (39–41). At the standard equilibrium temperature and pressure (STP), the chemical potential of hydrogen gas per mole at 1 atmosphere (STP) is described in Eqs (47–50) as follows:

$$\mu_{H}^{H_2} = \frac{1}{2}RT\ln\left(\frac{K_{H_2}}{K^o}\right), \tag{47}$$

where K_{H_2} denotes the hydrogen gas pressure in the atmosphere and K^o indicates 1 atmospheric pressure

$$\mu^{\beta}{}_{H(CH)}{}^{\beta} = \frac{\delta\Delta G^{\beta}{}_{CH}}{\delta_{CH}}, \tag{48}$$

$$\mu^{\alpha}{}_{H(CH)}{}^{\alpha} = \frac{\delta\Delta G^{\alpha}{}_{CH}}{\delta_{CH}}, \tag{49}$$

$$\mu^{\theta}{}_{H(CH)}{}^{\theta} = \frac{\delta\Delta G^{\theta}{}_{(CH)}}{\delta_{CH}}, \tag{50}$$

($\Delta G\alpha$), ($\Delta G\beta$), and ($\Delta G\theta$) represent the Gibbs free energies required for the phase transition in the system [145].

Adequate control of phase transitions for α, β, and θ hydrides in HEAs is important in determining how much hydrogen can be stored (Table 9), how fast it can be absorbed and desorbed, and how stable the materials remain over many cycles. Hence, due consideration of this phase transition will help in improving hydrogen storage performance [218,219].

Table 9. Phase transition [218,219].

	Phases	Storage capacity
1	α-Phase	Corresponds to dissolution of hydrogen in solid solution with limited hydrogen content, resulting in lower storage capacity.
2	β-Phase	The transition into β-phase, a metal hydride phase, indicates substantial hydrogen uptake with a higher hydrogen-to-metal ratio (H/M), enabling a high storage capacity.
3	θ-Phase	The phase indicates a complex hydride phase such as the Laves phase, which can store hydrogen density but may require higher activation energy and exhibit slower kinetics.
4	Reversibility and cycling stability	Reversible hydrogen storage depends on the ability of the alloys to transition between the phases without structural damage. HEAs with stable α-β transitions with a limited formation of brittle phases can sustain a better cycling performance with minimal capacity loss after many cycles.

4.1. Thermodynamic advantages of HEAs

Thermodynamics provides a fundamental framework for studying the interaction between hydrogen and HEAs. The high-entropy alloys exhibit a number of thermodynamic advantages over traditional alloys, including:

(a) High configurational entropy: The configurational entropy of these alloys is significantly higher than that of conventional alloys. This is because the large number of constituent elements in the alloys allows for a greater number of potential arrangements of atoms, leading to a higher degree of disorder. This high configurational entropy makes it more difficult for the alloy to undergo phase

transformations, which can lead to improved mechanical properties and greater resistance to corrosion and oxidation.

(b) HEAs usually exhibit enhanced solid solution strengthening due to the high entropy effect. This is because the large number of alloying elements in HEAs creates a high degree of lattice distortion, which enhances the interactions between the atoms and increases the strength of the alloy.

(c) Additionally, HEAs display improved high-temperature stability due to the formation of a single-phase microstructure. They also maintain superior mechanical properties at high temperatures due to the high configurational entropy and the enhanced solid solution strengthening.

(d) These materials have a wide range of applications, including aerospace, energy, and biomedical engineering, unlike traditional alloys, which often undergo phase separation or decomposition at high temperatures, leading to a loss of mechanical properties [220–222].

Figure 12, lists various advantages of thermodynamics as related to the HEAs. This information is vital for designing materials that can operate effectively under specific environmental conditions and for hydrogen storage and transport.

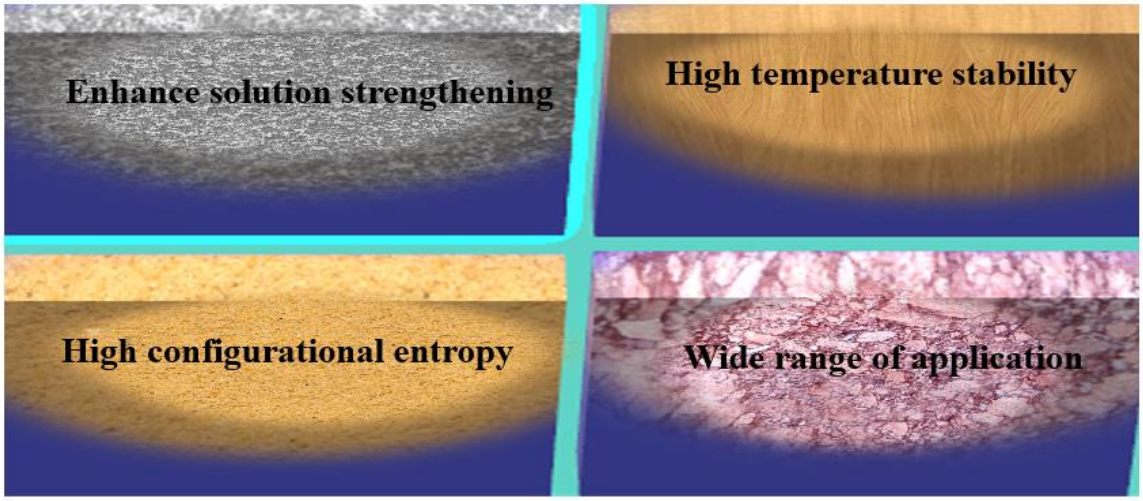

Figure 12. Thermodynamic advantages of HEAs [76,217].

5. Thermal analyses of hydrogenated-high entropy alloys

Thermal analysis is a valuable technique for investigating the thermal behavior of high-entropy alloys in various environmental conditions. This technique involves measuring the heat flow and temperature changes in a sample as it is subjected to thermal conditions, such as heating or cooling [223]. Figure 13, provides insights into the materials hydrogen absorption and desorption properties, including the reaction kinetics, reaction enthalpies, and thermodynamic stability of the hydride phases. Measuring the thermal effects on the interior parts of hydrogen storage components can be challenging. This is because convection involves complex fluid dynamics and heat transfer mechanisms that are difficult to quantify and model accurately [224]. In addition, to measuring thermal effects, simulation techniques can be used to predict and analyze the thermal behavior of hydrogen storage. These simulations typically involve the use of numerical models and computational fluid dynamics (CFD) techniques to simulate the flow of hydrogen gas and the resulting heat transfer within

the storage components [225]. Validating a simulation with experimental data is important to ensure accuracy and reliability [226]. The heat transfer between metal alloys and hydrogen gas primarily occurs through convection and conduction. This heat flows through the metal before it finally transfers to the hydrogen environment during exothermic and endothermic reactions. Consequently, it gives rise to thermal stress as such a thermal and structural analysis will be required using the parameters of temperature, heating rate, pressure, and linear dimension. The presence of impurities or surface oxides has an enormous impact on the anomalous temperature and prevents the hydrogen gas from diffusing into entropic alloys [227].

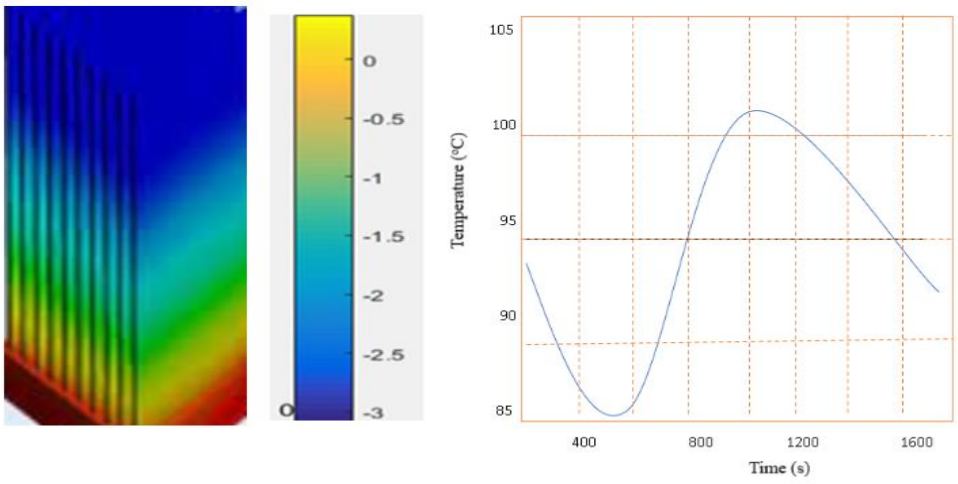

Figure 13. Thermal analyses of hydrogenated-high entropy alloys [227].

6. Embrittlement of structural alloys in the presence of hydrogen

The impact of hydrogen on metals and alloys is a topic of great importance in the energy sector, particularly in the storage and transportation of hydrogen. When hydrogen diffuses into HEAs, its atoms concentrate at grain boundaries, dislocations, and micro-voids, reducing cohesive strength and promoting crack nucleation and growth under stress. Hydrogen stabilizes cracks at the atomic scale by becoming entrapped in lattice imperfections, accelerating brittle fracture [228]. Furthermore, the presence of hydrogen in the HEA may increase dislocation mobility, causing localized deformation that concentrates stress and initiates cracks [229]. Phase transformation in brittle hydride phases can also cause embrittlement during hydrogen absorption. Lattice distortion, as mentioned earlier, enhances hydrogen solubility by creating interstitial sites with favorable energy levels, which further influences hydrogen's diffusion and concentration within the HEA's microstructure, impacting its mechanical properties [230].

As hydrogen atoms move through metal lattices, many factors influence their kinetic energy and may include temperature and pressure, as temperatures generally increase atomic mobility. As such, it increases the risk of hydrogen concentration in the HEA's structure and potentially increases the risk of hydrogen embrittlement. Additionally, freezing conditions can generate stresses in the metal structure, influencing its susceptibility to cracking. For instance, exposure of HEAs to freezing temperatures in the hydrogen environment can generate internal stress, which can build up and subsequently lead to small fractures. As a result, the hydrogen atoms remain within the alloy metals,

but their movement is reduced [231]. Moreover, an elevated hydrogen pressure can drive hydrogen atoms into a metal lattice, and increase the overall hydrogen concentration. This saturation enhances the availability of diffusion species within the interstitial site.

The change in pressure can alter the diffusion pathways. This alteration will affect the activation energy required for diffusion of the hydrogen atom and sometimes lower the activation energy by expanding the interstitial site. Under high-pressure, the hydrogen atom preferentially accumulates and becomes trapped in microstructural defects such as dislocation, grain boundaries, and vacancies [232]. This trapping site effectively reduces the mobility of hydrogen by holding atoms in place, thus, reducing the net diffusion rate despite increased overall concentration [233]. A notable example is the contribution made by Padmanabhan et al. [234] to the development of Ti–V–Cr–Mn–Mo–Ce HEA, synthesized via vacuum arc melting with cerium doping [234]. This HEA demonstrates unique hydrogen storage capabilities, up to a capacity of 3.63 wt.%. Additionally, it has potential for hydrogen embrittlement restraint. The interplay between temperature, pressure, hydrogen atom movement, and material integrity are therefore critical in assessing the long-term performance of HEAs in applications.

A nano-indentation technique is used to investigate the effects of diffusible hydrogen on materials at the atomic scale. This phenomenon provides information on failure mechanisms and corrosion effects [235]. The presence of hydrogen gas can influence the mechanical behavior of materials and their alloys and reduces the energy required for permanent deformation, making them harder when deformed [68,236]. Duarte et al. [235] analyzed the critical shear stress in hydrogen-rich environments using in-situ testing and multiscale simulations. High-entropy alloys were also investigated, and it was found that stresses were developed in both the soft and hard zones to increase yield strength and ductility. This property was obtained as a result of grain refinement to nano-scale and ultra-fine-grain structures [237]. A high fraction of grain boundaries can impact hydrogen diffusion and storage kinetics, which is one of the key components required in the design of materials for hydrogen storage and transportation [238].

Using TEM, high resolution imaging of fractures and crack morphology can be observed. In this case, a brittle feature will be revealed that might be associated with hydrogen embrittlement. The thickness of a TEM sample can range from 50–150 mm, the bright field and dark field TEM imaging may reveal dislocation structures, voids and twins related to embrittlement mechanism. For example, a high resolution can provide atomic-scale resolution of lattice distortions and twin boundaries formed due to hydrogen effects. Scanning TEM (STEM), together with EDS, can help in mapping the elemental distributions and hydrogen segregation indirectly [2–5]. For instance, the hydrogen embrittlement (HE) behavior of a CoCrFeMnNi HEA was investigated. Bright-field transmission electron microscopy (TEM) images revealed microbands with dislocations. Nevertheless, high-resolution TEM unveiled enlarged images of twinning and stacking fault (SF) bundles [239].

7. Exploring the safety, environmental, and economic aspects of HEAs in hydrogen storage

HEAs are considered solid-state hydrogen storage materials and inherently reduce leakage risks compared to traditional gaseous or liquid storage methods [240]. This is because hydrogen is absorbed into the alloy's lattice rather than existing as a free gas or liquid. The resulting solid hydrides provide mechanical integrity and pressure stability, thereby reducing the risk of bursts or ruptures commonly associated with high-pressure tanks [241]. The lattice distortion, a key characteristic of HEAs, further enhances hydrogen solubility by creating interstitial sites with favorable energy levels. The

multicomponent nature of HEAs also promotes stable phase structures under cyclic hydrogen loading, ensuring sustained pressure integrity over extended use [242]. Furthermore, HEAs operate at moderate pressures and near-ambient temperatures for hydrogen absorption and desorption, which reduces hazards compared to cryogenic or high-pressure systems. In the future, researchers should focus on the engineering integration of HEA storage units with safety monitoring, pressure relief, and containment systems to facilitate commercial deployment [243].

The environmental and economic implications of utilizing HEAs for hydrogen storage, as opposed to conventional alloys like $LaNi_5$ or MgH_2, are critical for future applications. HEAs that demonstrate efficient hydrogen storage capabilities under near-ambient conditions can diminish the energy needed for heating or pressurization, particularly when contrasted with MgH_2 [244]. As such, it necessitates high temperatures, enhancing the overall lifecycle environmental footprint. Nonetheless, the manufacturing of HEAs can be more intricate, involving multi-element melting and powder processing, potentially leading to a larger initial environmental footprint than that of simpler conventional alloys ($LaNi_5$ or MgH_2) [245]. Furthermore, HEAs often incorporate costly transitional metals or rare earths, which may increase raw material expenses relative to the more straightforward alloys like $LaNi_5$ or MgH_2 [246].

8. Conclusions

Hydrogen storage remains a major challenge that needs to be overcome for hydrogen to be widely adopted as a fuel source. Storing hydrogen in metal hydrides can be challenging as it requires high pressures and temperatures for hydrogen to be stored. This will make the process inefficient and potentially unsafe. The development of advanced materials for hydrogen storage is an active area of research. Therefore, scientists are exploring a range of options to identify materials that have a high hydrogen storage capacity, are lightweight, and are cost-effective. The use of high-entropy alloys for hydrogenation represents a promising approach to developing more effective and efficient materials for solid-state hydrogen storage. Because the HEAs exhibit a low melting temperature and high solubility, these features make them attractive for high-temperature applications. The greatest necessity for this progress is to embark on an effective method and develop new systems to navigate the vastness of compositional space. This will involve using computational tools, such as the CALPHAD, machine learning models, and high-throughput experimentation. As such, scientists can experiment with a wide variety of alloy compositions and conditions to improve the properties of the resulting materials. Nonetheless, only a few scientists have succeeded in modelling the hydrogenation of high-entropy alloys and their properties. Models of strains around misfit atoms in heterogeneous and homogeneous alloys were presented in this review, as was the principle of the thermodynamic process within metals and HEAs-hydrides. With this approach, the materials community will have a solid foundation and will be able to fully utilize the potential of HEAs for hydrogen storage. Alloy design and synthesis are of great importance as they can facilitate the manufacturing process and aid in the technological development of hydrogen storage. These approaches would strengthen the links between material development and fabrication techniques. Compared to conventional alloys, the components produced will exhibit excellent physical and mechanical properties. A variety of computational tools are being used to explore the alloy parameters and determine some relationships between them. Among the HEAs are the BCC crystal structures that have high volumetric and gravimetric storage capacities for hydrogen, while lightweight metals such as magnesium have a high capacity for kinetic hydrogen

absorption and desorption, and their composition can be modified to suit the specific purpose of any given condition. Additionally, more phases are formed due to an increase in the alloy composition, and this follows the rules of Gibbs phases. Moreover, if these HEAs contain intermetallic compounds, the formation will be more rapid. At equilibrium, the formation of this compound will be promoted depending on the enthalpy. Finally, the search for improved hydrogen storage systems remains a constantly developing field of research, with opportunities abounding to discover new materials that exhibit promising hydrogenation properties.

Use of AI tools declaration

The author declares he has not used Artificial Intelligence (AI) tools in the creation of this article.

Acknowledgment

The authors would like to sincerely thank the Centre for Surface Engineering Research Lab and Tshwane University of Technology for making available their resources in the course of this study.

Conflict of interest

The authors declare that the review paper was written in the absence of any commercial or financial relationships that could be construed as a potential conflict of interest.

Author contributions

Adebayo Ogunyinka contributed to the conceptualization, critical investigation, and writing of the original draft. Patricia Popoola and Olawale Popoola contributed to the administrative activity, resources, supervision, writing the review, and editing. Sadiku Rotimi contributed to the administrative activity, resources, supervision, writing the review, and editing. Sisa Pityana contributed to the administrative activity, resources, supervision, writing the review, and editing, while Modupeola Dada focused specifically on editing the review.

References

1. Rusman NAA, Dahari M (2016) A review on the current progress of metal hydrides material for solid-state hydrogen storage applications *Int J Hydrogen Energy* 41: 12108–12126. https://doi.org/10.1016/j.ijhydene.2016.05.244
2. Hirscher M (2010) Handbook of hydrogen storage: New materials for future energy storage. 1 Eds., Wiley. https://doi.org/10.1002/9783527629800
3. Yadav SK, Kumar TP, Verma A (2022) High-Entropy alloys for solid hydrogen storage: Potentials and prospects. *Trans Indian Natl Acad Eng* 7: 147–156. https://doi.org/10.1007/s41403-021-00316-w
4. Yartys VA, Lototskyy MV (2022) Laves type intermetallic compounds as hydrogen storage materials: A review. *J Alloys Compd* 916: 165219. https://doi.org/10.1016/j.jallcom.2022.165219

5. Hassan IA, Ramadan HS, Saleh MA, et al. (2021) Hydrogen storage technologies for stationary and mobile applications: Review, analysis and perspectives. *Renewable Sustainable Energy Rev* 149: 111311. https://doi.org/10.1016/j.rser.2021.111311
6. Tarasov BP, Fursikov PV, Volodin AA, et al. (2021) Metal hydride hydrogen storage and compression systems for energy storage technologies. *Int J Hydrogen Energy* 46: 13647–13657. https://doi.org/10.1016/j.ijhydene.2020.07.085
7. Kalibek MR, Ospanova AD, Suleimenova B, et al. (2024) Solid-state hydrogen storage materials. *Discover Nano* 19: 195. https://doi.org/10.1186/s11671-024-04137-y
8. Ge YT (2024) Characterisation of pressure-concentration-temperature profiles for metal hydride hydrogen storage alloys with model development. *Energy Storage* 6: 504. https://doi.org/10.1002/est2.504
9. Kim H, Faisal M, Lee SI, et al. (2021) Activation of Ti–Fe–Cr alloys containing identical AB_2 fractions. *J Alloys Compd* 864: 158876. https://doi.org/10.1016/j.jallcom.2021.158876
10. Weadock NJ, Voorhees PW, Fultz B (2021) Interface pinning causes the hysteresis of the hydride transformation in binary metal hydrides. *Phys Rev Mater* 5: 013604. https://doi.org/10.1103/PhysRevMaterials.5.013604
11. Qureshi T, Khan MM, Pali HS (2024) The future of hydrogen economy: Role of high entropy alloys in hydrogen storage. *J Alloys Compd* 1004: 175668. https://doi.org/10.1016/j.jallcom.2024.175668
12. Halpren E, Yao X, Chen ZW, et al. (2024) Machine learning assisted design of BCC high entropy alloys for room temperature hydrogen storage. *Acta Mater* 270: 119841. https://doi.org/10.1016/j.actamat.2024.119841
13. Lu Z, Huang Z, Wang H, et al. (2025) Construction of disordered interfaces in high-entropy alloy multilayer films through atomic-scale interactions to enhance hydrogen storage properties. *J Alloys Compd* 1037: 182243. https://doi.org/10.1016/j.jallcom.2025.182243
14. Zhang X, Lou Z, Gao M, et al. (2024) Metal hydrides for advanced hydrogen/lithium storage and ionic conduction applications. *Acc Mater Res* 5: 371–384. https://doi.org/10.1021/accountsmr.3c00267
15. Gao MC, Miracle DB, Maurice D, et al. (2018) High-entropy functional materials. *J Mater Res* 33: 3138–3155. https://doi.org/10.1557/jmr.2018.323
16. Marques F, Balcerzak M, Winkelmann F, et al. (2021) Review and outlook on high-entropy alloys for hydrogen storage. *Energy Environ Sci* 14: 5191–5227. https://doi.org/10.1039/D1EE01543E
17. Lototskyy MV, Yartys VA, Pollet BG, et al. (2014) Metal hydride hydrogen compressors: A review. *Int J Hydrogen Energy* 39: 5818–5851. https://doi.org/10.1016/j.ijhydene.2014.01.158
18. Altaf M, Demirci UB, Haldar AK (2025) Review of solid-state hydrogen storage: Materials categorization, recent developments, challenges and industrial perspectives. *Energy Rep* 13: 5746–5772. https://doi.org/10.1016/j.egyr.2025.05.034
19. Du YL, Sun ZY, Fu BA, et al. (2025) Unleashing the power of hydrogen: Challenges and solutions in solid-state storage. *Int J Hydrogen Energy* 136: 1112–1123. https://doi.org/10.1016/j.ijhydene.2025.02.445
20. Lenis JA, Velandia JA, Ocampo RA, et al. (2025) Challenges and potential future trends on high entropy alloy for solid hydrogen storage: Systematic review. *J Power Sources* 656: 238011. https://doi.org/10.1016/j.jpowsour.2025.238011

21. Witman M, Ek G, Ling S, et al. (2021) Data-driven discovery and synthesis of high entropy alloy hydrides with targeted thermodynamic stability. *Chem Mater* 33: 4067–4076. https://doi.org/10.1021/acs.chemmater.1c00647
22. Abdalla AM, Hossain S, Nisfindy OB, et al. (2018) Hydrogen production, storage, transportation and key challenges with applications: A review. *Energy Convers Manag* 165: 602–627. https://doi.org/10.1016/j.enconman.2018.03.088
23. Züttel A, Remhof A, Borgschulte A, et al. (2010) Hydrogen: The future energy carrier. *Philos Trans R Soc A* 368: 2010. https://doi.org/10.1098/rsta.2010.0113
24. Huang J, Yang W, Gao Z, et al. (2025) Heterostructured multi-principal element alloys prepared by laser-based techniques. *Microstructures* 5: 1–32. https://doi.org/10.20517/microstructures.2024.86
25. Cantor B (2021) Multicomponent high-entropy Cantor alloys. *Prog Mater Sci* 120: 100754. https://doi.org/10.1016/j.pmatsci.2020.100754
26. Körmann F, Kostiuchenko T, Shapeev A, et al. (2021) B2 ordering in body-centered-cubic AlNbTiV refractory high-entropy alloys. *Phys Rev Mater* 5: 053803. https://doi.org/10.1103/PhysRevMaterials.5.053803
27. Wang S (2013) Atomic structure modeling of multi-principal-element alloys by the principle of maximum entropy. *Entropy* 15: 5536–5548. https://doi.org/10.3390/e15125536
28. Hong H, Guo H, Cui Z, et al. (2024) Structure modification of magnesium hydride for solid hydrogen storage. *Int J Hydrogen Energy* 78: 793–804. https://doi.org/10.1016/j.ijhydene.2024.06.327
29. Wang L, Liu W, Zhu B, et al. (2021) Influences of strain rate, Al concentration and grain heterogeneity on mechanical behavior of $CoNiFeAl_xCu_{1-x}$ high-entropy alloys: A molecular dynamics simulation. *J Mater Res Technol* 14: 2071–2084 https://doi.org/10.1016/j.jmrt.2021.07.116
30. Zhang Y, Lu ZP, Ma SG, et al. (2014) Guidelines in predicting phase formation of high-entropy alloys. *MRS Commun* 4: 57–62. https://doi.org/10.1557/mrc.2014.11
31. Bulavchenko OA, Vinokurov ZS (2023) In situ X-ray diffraction as a basic tool to study oxide and metal oxide catalysts. *Catalysts* 13: 1421. https://doi.org/10.3390/catal13111421
32. Morin L, Braham C, Tajdary P, et al. (2021) Reconstruction of heterogeneous surface residual-stresses in metallic materials from X-ray diffraction measurements. *Mech Mater* 158: 103882. https://doi.org/10.1016/j.mechmat.2021.103882
33. Wu Z, Bei H, Otto F, et al. (2014) Recovery, recrystallization, grain growth and phase stability of a family of FCC-structured multi-component equiatomic solid solution alloys. *Intermetallics* 46: 131–140. https://doi.org/10.1016/j.intermet.2013.10.024
34. Bahmani A, Lotfpour M, Taghizadeh M, et al. (2022) Corrosion behavior of severely plastically deformed Mg and Mg alloys. *J Magnes Alloy* 10: 2607–2648. https://doi.org/10.1016/j.jma.2022.09.007
35. Moschetti M, Burr PA, Obbard E, et al. (2022) Design considerations for high entropy alloys in advanced nuclear applications. *J Nucl Mater* 567: 153814. https://doi.org/10.1016/j.jnucmat.2022.153814
36. Purdy GR, Kirkaldy JS (1971) Homogenization by diffusion. *Springer Metall Trans* 2: 371–378. https://doi.org/10.1007/BF02663324

37. Murty BS, Yeh JW, Ranganathan S, et al. (2019) 5—Alloy design in the 21st century: ICME, materials genome, and artificial intelligence strategies. *High-Entropy Alloys* 2019: 81–101. https://doi.org/10.1016/B978-0-12-816067-1.00005-9
38. Smith RL, Phoenix SL (1981) Asymptotic distributions for the failure of fibrous materials under series-parallel structure and equal load-sharing. *J Appl Mech* 48: 1–8. https://doi.org/10.1115/1.3157595
39. Cai J, Chu X, Xu K, et al. (2020) Machine learning-driven new material discovery. *Nanoscale Adv* 2: 3115–3130. https://doi.org/10.1039/D0NA00388C
40. Kaushik N, Meena A, Mali HS (2022) High entropy alloy synthesis, characterisation, manufacturing & potential applications: A review. *Mater Manuf Processes* 37: 1085–1109. https://doi.org/10.1080/10426914.2021.2006223
41. Dangwal S, Ikeda Y, Grabowski B, et al. (2024) Machine learning to explore high-entropy alloys with desired enthalpy for room-temperature hydrogen storage: Prediction of density functional theory and experimental data. *Chem Eng J* 493: 152606. https://doi.org/10.1016/j.cej.2024.152606
42. Kumar A, Kumar S, Kumar A, et al. (2023) Structural phase transformation in single-crystal Fe-Cr-Ni alloy during creep deformation using molecular dynamics simulation and regression-based machine learning methodology. *Bull Mater Sci* 47: 1–11. https://doi.org/10.1007/s12034-023-03075-2
43. Smith ER, Theodorakis PE (2024) Multiscale simulation of fluids: coupling molecular and continuum. *R Soc Chem* 26: 724–744. https://doi.org/10.1039/D3CP03579D
44. Komanduri R, Chandrasekaran N, Raff LM (2000) Molecular dynamics simulation of atomic-scale friction. *Phys Rev B* 61: 14007. https://doi.org/10.1103/PhysRevB.61.14007
45. Cheng B, Kong L, Cai H, et al (2024). Pushing the Boundaries of solid-state hydrogen storage: A refined study on TiVNbCrMo high-entropy alloys. *Int J Hydrogen Energy* 60: 282–292. https://doi.org/10.1016/j.ijhydene.2024.02.192
46. Sorkin V, Chen S, Tan TL, et al. (2021) First-principles-based high-throughput computation for high entropy alloys with short range order. *J Alloys Compd* 882: 160776. https://doi.org/10.1016/j.jallcom.2021.160776
47. Ferrin P, Kandoi S, Nilekar AU, et al. (2012) Hydrogen adsorption, absorption and diffusion on and in transition metal surfaces: A DFT study. *Surf Sci* 606: 679–689. https://doi.org/10.1016/j.susc.2011.12.017
48. Zhang Z, Mansouri Tehrani A, Oliynyk AO, et al. (2021) Finding the next super hard material through ensemble learning. *Adv Mater* 33: 2005112. https://doi.org/10.1002/adma.202005112
49. Hu J, Zhang J, Xiao H, et al. (2020) A density functional theory study of the hydrogen absorption in high entropy alloy TiZrHfMoNb. *Inorg Chem* 59: 9774–9782. https://doi.org/10.1021/acs.inorgchem.0c00989
50. Hensley AJ, Ghale K, Rieg C, et al. (2017) DFT-based method for more accurate adsorption energies: An adaptive sum of energies from RPBE and vdw density functionals. *J Phys Chem C* 121: 4937–4945. https://doi.org/10.1021/acs.jpcc.6b10187
51. Zheng W, Wu L, Shuai Q, et al. (2024) Mechanism for adsorption, dissociation, and diffusion of hydrogen in high-entropy alloy AlCrTiNiV: First-Principles calculation. *Nanomaterials* 14: 1391. https://doi.org/10.3390/nano14171391

52. Ghosh PS, Ali K, Arya A, et al. (2024) Efficient screening of single phase forming low-activation high entropy alloys. *J. Alloys Compd* 978: 173172. https://doi.org/10.1016/j.jallcom.2023.173172
53. Khan W, Masood MK, et al. (2024) The investigation of rubidium-based hydrides for hydrogen storage application: Density functional theory study. *Mater Sci Semicond Process* 173: 108149. https://doi.org/10.1016/j.mssp.2024.108149
54. Fan Q, Hou H, Yang J, et al. (2024) Effect of pressures on the structural, electronic, optical, elastic, dynamical properties and thermal properties of Mo_2C: A study explored by theoretical simulation. *Int J Refract Met Hard Mater* 119: 106522. https://doi.org/10.1016/j.ijrmhm.2023.106522
55. Zhao L, Jiang L, Yang LX, et al. (2022) High throughput synthesis enabled exploration of CoCrFeNi-based high entropy alloys. *J Mater Sci Technol* 110: 269–282. https://doi.org/10.1016/j.jmst.2021.09.031
56. Wan W, Liang K, Zhu P, et al. (2024) Recent advances in the synthesis and fabrication methods of high-entropy alloy nanoparticles. *J Mater Sci Technol* 178: 226–246. https://doi.org/10.1016/j.jmst.2023.08.051
57. Cortis D, Pilone D, Grazzi F, et al. (2025) Functionally graded material via L-PBF: Characterisation of multi-material junction between steels (AISi316L/16MnCr5), copper (CuCrZr) and aluminium alloys (Al-Sc/$AlSi_{10}Mg$). *Prog Addit Manuf* 10: 2455–2472. https://doi.org/10.1007/s40964-024-00761-3
58. Kim KS, Couillard M, Tang Z, et al, (2024) Continuous synthesis of high-entropy alloy nanoparticles by in-flight alloying of elemental metals. *Nat Commun* 15: 1450. https://doi.org/10.1038/s41467-024-45731-z
59. Ron T, Shirizly A, Aghion E (2023) Additive manufacturing technologies of High Entropy Alloys (HEA): Review and Prospects. *Materials* 16: 2454. https://doi.org/10.3390/ma16062454
60. Jain S, Kumar V, Samal S (2024) Predicting the effect of Ta on the mechanical behaviour and experimental validation of novel six component Fe-Co-Ni-Cr-V-Ta eutectic high entropy alloys. *Int J Refract Met Hard Mater* 120: 106572. https://doi.org/10.1016/j.ijrmhm.2024.106572
61. Shivam V, Basu J, Shadangi Y, et al. (2018) Mechano-chemical synthesis, thermal stability and phase evolution in AlCoCrFeNiMn high entropy alloy. *J Alloys Compd* 757: 87–97. https://doi.org/10.1016/j.jallcom.2018.05.057
62. Vaidya M, Pradeep KG, Murty BS, et al. (2017) Radioactive isotopes reveal a non sluggish kinetics of grain boundary diffusion in high entropy alloys. *Sci Rep* 7: 12293. https://doi.org/10.1038/s41598-017-12551-9
63. Ikeda Y, Grabowski B, Körmann F (2019) Ab initio phase stabilities and mechanical properties of multicomponent alloys: A comprehensive review for high entropy alloys and compositionally complex alloys. *Mater Charact* 147: 464–511. https://doi.org/10.1016/j.matchar.2018.06.019
64. Rhode M, Wetzel A, Ozcan O, et al. (2020) Hydrogen diffusion and local Volta potential in high- and medium-entropy alloys. *In IOP Conference Series: Materials Science and Engineering* 882: 012015. IOP Publishing. https://doi.org/10.1088/1757-899X/882/1/012015
65. Qiu J, Yang Y, Wan H, et al. (2025) Interface-Engineered TiV Bimetal catalysts with synergistic effects for enhancing hydrogen storage performance in Mg–Ni-Based material. *J Phy Chem Lett* 16: 8084–8091. https://doi.org/10.1021/acs.jpclett.5c01248
66. Sharma B, Harini S (2019) A possibility of Pd based high entropy alloy for hydrogen gas sensing applications. *Mater Res Express* 6: 1165d7. https://doi.org/10.1088/2053-1591/ab4fae.

67. Hirscher M, Yartys VA, Baricco M, et al. (2020) Materials for hydrogen-based energy storage—past, recent progress and future outlook. *J Alloys Compd* 827: 153548. https://doi.org/10.1016/j.jallcom.2019.153548
68. Pu Z, Chen Y, Dai LH (2018) Strong resistance to hydrogen embrittlement of high-entropy alloy *Mater Sci Eng A* 736: 2018. https://doi.org/10.1016/j.msea.2018.08.101
69. Duan Y, Li Z, Liu X, et al. (2022) Optimized microwave absorption properties of FeCoCrAlGdx high-entropy alloys by inhibiting nanograin coarsening. *J Alloys Compd* 921: 166088. https://doi.org/10.1016/j.jallcom.2022.166088
70. Li Y, Feng Z, Hao L, et al. (2020). A review on functionally graded materials and structures via additive manufacturing: from multi-scale design to versatile functional properties. *Adv Mater Technol* 5: 1900981. https://doi.org/10.1002/admt.201900981
71. DebRoy T, Mukherjee T, Wei HL, et al. (2021) Metallurgy, mechanistic models and machine learning in metal printing. *Nat Rev Mater* 6: 48–68. https://doi.org/10.1038/s41578-020-00236-1
72. Chen B, Zhuo L (2023) Latest progress on refractory high entropy alloys: Composition, fabrication, post processing, performance, simulation and prospect. *Int J Refract Met Hard Mater* 110: 105993. https://doi.org/10.1016/j.ijrmhm.2022.105993
73. Sakaki K, Kim H, Asano K, et al. (2020). Hydrogen storage properties of Nb-based solid solution alloys with a BCC structure. *J Alloys Compd* 820: 53399. https://doi.org/10.1016/j.jallcom.2019.153399
74. Kong L, Cheng B, Wan D, et al. (2023) A review on BCC-structured high-entropy alloys for hydrogen storage. *Front Mater* 10: 1135864. https://doi.org/10.3389/fmats.2023.1135864
75. Floriano R, Zepon G, Edalati K, et al. (2021) Hydrogen storage properties of new A_3B_2-type TiZrNbCrFe high-entropy alloy. *Int J Hydrogen Energy* 46: 23757–23766. https://doi.org/10.1016/j.ijhydene.2021.04.181
76. Gorr B, Azim M, Christ HJ, et al. (2015) Phase equilibria, microstructure, and high temperature oxidation resistance of novel refractory high-entropy alloys. *J Alloys Compd* 624: 270–278. https://doi.org/10.1016/j.jallcom.2014.11.012
77. Melnick AB, Soolshenko VK (2017) Thermodynamic design of high-entropy refractory alloys. *J Alloys Compd* 694: 223–227. https://doi.org/10.1016/j.jallcom.2016.09.189
78. Fukai Y (1984) Site preference of interstitial hydrogen in metals. *J Less Common Met* 101: 1–16. https://doi.org/10.1016/0022-5088(84)90084-5
79. Hu J, Zhang J, Li M, et al. (2022) The origin of anomalous hydrogen occupation in high entropy alloys. *J Mater Chem A* 10: 7228–7237. https://doi.org/10.1039/D1TA10649J
80. Ghotia S, Kumar P, Srivastava AK (2025) A review on 2D materials: unveiling next-generation hydrogen storage solutions, advancements and prospects. *J Mater Sci* 60: 1071–1097. https://doi.org/10.1007/s10853-024-10054-3
81. Hu J, Zhang J, Xiao H, et al. (2021) A first-principles study of hydrogen storage of high entropy alloy TiZrVMoNb. *Inter J Hydrogen Energy* 46: 21050–21058. https://doi.org/10.1016/j.ijhydene.2021.03.200
82. Luo H, Li Z, Raabe D (2017) Hydrogen enhances strength and ductility of an equiatomic high-entropy alloy. *Sci Rep* 7: 9892. https://doi.org/10.1038/s41598-017-10774-4
83. Radhika N, Niketh MS, Akhil UV, et al. (2024) High entropy alloys for hydrogen storage applications: A machine learning-based approach. *Results Eng* 23: 102780. https://doi.org/10.1016/j.rineng.2024.102780

84. Kattner UR (2016) The CALPHAD method and its role in material and process development. *Tecnol Metal Mater e Mineração* 13: 3–15. https://doi.org/10.4322/2176-1523.1059
85. Liu ZK, Wang Y (2016) Computational thermodynamics of materials. *Cambridge University Press*. https://doi.org/10.1017/cbo9781139018265
86. Cho Y, Cho H, Cho ES (2023) Nanointerface engineering of metal hydrides for advanced hydrogen storage. *Chem Mater* 35: 366–385. https://doi.org/10.1021/acs.chemmater.2c02628
87. Ghassemali E, Conway PLJ (2022) High-throughput CALPHAD: A powerful tool towards accelerated metallurgy. *Front Mater* 9: 889771. https://doi.org/10.3389/fmats.2022.889771
88. Zhu S, Sarıtürk D, Arróyave R (2025) Accelerating CALPHAD-based phase diagram predictions in complex alloys using universal machine learning potentials: Opportunities and challenges. *Acta Mater* 286: 120747. https://doi.org/10.1016/j.actamat.2025.120747
89. Hasan S, Adhikari P, San S, et al. (2025) Phase stability, electronic, mechanical, lattice distortion, and thermal properties of complex refractory-based high entropy alloys TiVCrZrNbMoHfTaW with varying elemental ratios. *RSC Adv* 15: 1878–1895. https://doi.org/10.1039/d4ra07460b
90. Wang X, Guo W, Fu Y (2021) High-entropy alloys: Emerging materials for advanced functional applications. *J Mater Chem A* 9: 663–701. https://doi.org/10.1039/D0TA09601F
91. Moussa M, van Eijck L, Huot J, et al. (2025) Structure analysis (XRD and Neutrons) and hydrogen storage properties of Hf1-xTixNbVZr BCC high entropy alloys. *J Alloys Compd* 1010: 177103. https://doi.org/10.1016/j.jallcom.2024.17710
92. Lee C, Chou Y, Kim G, et al. (2020) Lattice-distortion-enhanced yield strength in a refractory high-entropy alloy. *Adv Mater* 32: 2004029. https://doi.org/10.1002/adma.202004029
93. Somo TR, Lototskyy MV, Yartys VA, et al. (2023) Hydrogen storage behaviors of high entropy alloys: a Review. *J Energy Storage* 73: 108969. https://doi.org/10.1016/j.est.2023.108969
94. Singh A, Kumari P, Sahoo SK, et al. (2025) Studies on hydrogen storage properties of TiVFeNi, $(TiVFeNi)_{95}Zr_5$ and $(TiVFeNi)_{90}Zr_{10}$ high entropy alloys. *Int J Hydrogen Energy* 141: 738–749. https://doi.org/10.1016/j.ijhydene.2024.09.064
95. Huang C, Ke H, Wang L, et al. (2025) Design and characterization of TiZrNb-M (M = Fe, Co, Ni) eutectic multi-component alloys. *Mater Charact* 224: 114991. https://doi.org/10.1016/j.matchar.2025.114991
96. Zhang J, Zhang H, Xiong J, et al. (2025) Anomalous component-dependent lattice thermal conductivity in MoWTaTiZr refractory high-entropy alloys. *iScience* 28: 112100 https://doi.org/10.1016/j.isci.2025.112100
97. Sheng GUO, Liu CT (2011) Phase stability in high entropy alloys: Formation of solid-solution phase or amorphous phase. *Prog Nat Sci Mater Int* 21: 433–446. https://doi.org/10.1016/S1002-0071(12)60080-X
98. Keith A, Zlotea C, Szilágyi PÁ (2023) Perspective of interstitial hydrides of high-entropy alloys for vehicular hydrogen storage. *Int J Hydrogen Energy* 52: 531–546. https://doi.org/10.1016/j.ijhydene.2023.01.141
99. Hu HZ, Zhang XX, Li SS, et al. (2025) A review of body-centred cubic-structured alloys for hydrogen storage: composition, structure, and properties: A review of body-centred cubic-structured alloys for hydrogen storage. *Rare Metals* 44: 1497–1521. https://doi.org/10.1007/s12598-024-02994-1

100. Praveen S, Murty BS, Kottada RS (2012) Alloying behavior in multi-component AlCoCrCuFe and NiCoCrCuFe high entropy alloys. *Mater Sci Eng A* 534: 83–89. https://doi.org/10.1016/j.msea.2011.11.044
101. Singh AK, Subramaniam A (2014) On the formation of disordered solid solutions in multi-component alloys. *J Alloys Compd* 587: 113–119. https://doi.org/10.1016/j.jallcom.2013.10.133
102. Yadav YK, Shaz MA, Mukhopadhyay NK, et al. (2025) High entropy alloys synthesized by mechanical alloying: A review. *J Alloys Metall Syst* 9: 100170. https://doi.org/10.1016/j.jalmes.2025.100170
103. Huot J, Ravnsbæk DB, Zhang J, et al. (2013) Mechanochemical synthesis of hydrogen storage materials. *Prog Mater Sci* 58: 30–75. https://doi.org/10.1016/j.pmatsci.2012.07.001
104. Villaça JC, da Silva LCR, Locatelli FR, et al. (2020) Full-factorial design for statistical planning of attritor milling parameters and evaluation of effects on particle size and structure of sodium-montmorillonite. *Eng Res Express* 2: 015050. https://doi.org/10.015050.10.1088/2631-8695/ab7d85
105. Aliyu, A, Srivastava C (2021) Microstructure and electrochemical properties of FeNiCoCu medium entropy alloy-graphene oxide composite coatings. *J Alloys Compd* 864: 158851. https://doi.org/10.1016/j.jallcom.2021.158851
106. Canakci A, Erdemir F, Varol T, et al. (2013) Determining the effect of process parameters on particle size in mechanical milling using the Taguchi method: Measurement and analysis. *Measurement* 46: 3532–3540. https://doi.org/10.1016/j.measurement.2013.06.035
107. Yadav TP, Kumar A, Verma SK, et al. (2022) High-entropy alloys for solid hydrogen storage: potentials and prospects. *Trans Indian Natl Acad Eng* 7: 147–156. https://doi.org/10.1007/s41403-021-00316-w
108. Palumbo O, Carboni N, Trequattrini F, et al. (2022) Mechanochemical synthesis and hydrogen sorption properties of a V-Ni alloy. *Hydrogen* 3: 112–122. https://doi.org/10.3390/hydrogen3010009
109. Sleiman S, Huot J (2022) Microstructure and first hydrogenation properties of $TiHfZrNb_{1-x}V_{1+x}$ Alloy for x = 0, 0.1, 0.2, 0.4, 0.6 and 1. *Molecules* 27: 1054. https://doi.org/10.3390/molecules27031054
110. Xu X, Zhang B, Shi F, et al. (2025) Study on the Influence of hygrothermal aging on the mechanical properties of carbon fabric/poly-etherether-ketone Composites. *Polymers* 17: 724. https://doi.org/10.3390/polym17060724
111. Feng Z, Zhong H, Li D, et al. (2022) Microstructure and hydrogen storage properties of Ti-V-Mn alloy with Zr, Ni, and Zr_7 Ni_{10} addition. *J Mater Res* 37: 591–1601. https://doi.org/10.1557/s43578-022-00555-9
112. Balcerzak M (2018) Effect of Ni on electrochemical and hydrogen storage properties of V-rich body-centered-cubic solid solution alloys. *Int J Hydrogen Energy* 43: 8395–8403. https://doi.org/10.1016/j.ijhydene.2018.03.123
113. Zhang Y, Li R, Cong M, et al. (2022) Effect of hypo-stoichiometry on microstructure and hydrogenation behaviours of multiphase $ZrTi_{0.1}V_{2-x}$ alloys. *Intermetallic* 142: 107464. https://doi.org/10.1016/j.intermet.2022.107464
114. Le TH, Kim MP, Park CH, et al. (2024) Recent developments in materials for physical hydrogen storage: a review. *Materials* 17: 666. https://doi.org/10.3390/ma17030666

115. Hou Z, Guo S, Zhang X, et al. (2025) Hydrogen storage and stability of rare earth-doped TiFe alloys under extensive cycling. *Int J Hydrogen Energy* 136: 469–476. https://doi.org/10.1016/j.ijhydene.2025.05.043
116. Shi H, Sun XY, Zeng SP, et al. (2023) Nano-porous nonprecious high-entropy alloys as multisite electrocatalysts for ampere-level current-density hydrogen evolution. *Small Struct* 4: 2300042. https://doi.org/10.1002/sstr.202300042
117. Dematteis EM, Berti N, Cuevas F, et al. (2021) Substitutional effects in TiFe for hydrogen storage: A comprehensive review. *Mater Adv* 8: 2524–2560. https://doi.org/10.1039/D1MA00101A
118. Mohammadi A, Ikeda Y, Edalati P, et al. (2022) High-entropy hydrides for fast and reversible hydrogen storage at room temperature: Binding-energy engineering via first-principles calculations and experiments. *Acta Mater* 236: 118117. https://doi.org/10.1016/j.actamat.2022.118117
119. Zhang YH, Gong PF, Li LW, et al. (2019) Hydrogen storage thermodynamics and dynamics of La–Mg–Ni-based $LaMg_{12}$-type alloys synthesized by mechanical milling. *Rare Met* 38: 1144–1152. https://doi.org/10.1007/s12598-016-0842-0
120. Jeyaraman S, Danilov DL, Notten PH, et al. (2025) Influence of Ni and Nb addition in TiVCr-based high entropy alloys for room-temperature hydrogen storage. *Energies* 18: 3920. https://doi.org/10.3390/en18153920
121. Liu Y, Wang F, Cao Y, et al. (2010) Mechanisms for the enhanced hydrogen desorption performance of the TiF4-catalyzed Na_2LiAlH_6 used for hydrogen storage. *Energy Environ Sci* 3: 645–653. https://doi.org/10.1039/B920270F
122. Nygård MM, Ek G, Karlsson D, et al. (2019) Counting electrons-a new approach to tailor the hydrogen sorption properties of high-entropy alloys. *Acta Mater* 175: 121–129. https://doi.org/10.1016/j.actamat.2019.06.002
123. Shahi RR, Gupta AK, Kumari P (2022) Perspectives of high entropy alloys as hydrogen storage materials. *Int J Hydrogen Energy* 48: 21412–21428. https://doi.org/10.1016/j.ijhydene.2022.02.113
124. Chen H, Zhao Z, Xiang H, et al. (2020) Effect of reaction routes on the porosity and permeability of porous high entropy $(Y_{0.2}Yb_{0.2}Sm_{0.2}Nd_{0.2}Eu_{0.2})$ B_6 for transpiration cooling. *J Mater Sci Technol* 38: 80–85. https://doi.org/10.1016/j.jmst.2019.09.006
125. Galey B, Batalha N, Auroux A (2023) Thermal analysis and solid-state hydrogen storage: Mg/MgH_2 system case study. *Therm Anal Calorim*. https://doi.org/10.1515/9783110590449-003
126. Zafar S, Khan A (2023) Integrated hydrogen fuel cell power system as an alternative to diesel-electric power system for conventional submarines. *Int J Hydrogen Energy* 51: 1560–1572. https://doi.org/10.1016/j.ijhydene.2023.08.370
127. Behera A (2021) *Advanced materials: An introduction to modern materials science*. 1 Eds, *Springer Cham*, 748. https://doi.org/10.1007/978-3-030-80359-9
128. Kaushal J, Chowdhury SPD (2025) Hydrogen-powered fuel cell integration in low voltage microgrid systems: performance evaluation and power quality analysis. *Int J Ambient Energy* 46: 2446524. https://doi.org/10.1080/01430750.2024.2446524
129. Zhou Y, Dan Z (2025) Modern energy resilience studies with artificial intelligence for energy transitions. *Cell Rep Phys Sci* 6: 102508. https://doi.org/10.1016/j.xcrp.2025.102508

130. Yang F, Wang J, Zhang Y, et al. (2022) Recent progress on the development of high entropy alloys (HEAs) for solid hydrogen storage: A review. *Int J Hydrogen Energy* 47: 11236–11249. https://doi.org/10.1016/j.ijhydene.2022.01.141
131. Yang C, Gao Y, Ma T, et al. (2023) Metal alloys-structured electrocatalysts: metal-metal interactions, coordination microenvironments, and structural property-reactivity relationships. *Adv Mater* 35: 2301836. https://doi.org/10.1002/adma.202301836
132. Yi J, Zhang S, Zhu D, et al. (2025) Mitigating hydrogen embrittlement in CoCrNi alloy using a self-refilling nanoscale amorphous oxide layer. *Corros Sci* 251: 112941. https://doi.org/10.1016/j.corsci.2025.112941
133. Amiri A, Shahbazian-Yassar R (2023) Correction: Recent progress of high-entropy materials for energy storage and conversion. *J Mater Chem A* 11: 1512–1512. https://doi.org/10.1039/D2TA90294J
134. Zlotea C, Bouzidi A, Montero J, et al. (2022) Compositional effects on the hydrogen storage properties in a series of refractory high entropy alloys. *Front Energy Res*, 10. https://doi.org/10.3389/fenrg.2022.991447
135. Ma N, Zhao W, Wang W, et al. (2024) Large scale of green hydrogen storage: Opportunities and challenges. *Int J Hydrogen Energy* 50: 379–396. https://doi.org/10.1016/j.ijhydene.2023.09.021
136. Dematteis EM, Amdisen MB, Autrey T, et al. (2022) Hydrogen storage in complex hydrides: Past activities and new trends. *Prog Energy* 4: 032009. https://doi.org/10.1088/2516-1083/ac7499
137. Miedema AR, Buschow KHJ, Van Mal HH (1976) Which intermetallic compounds of transition metals form stable hydrides . *J Less Common Met* 49: 463–472. https://doi.org/10.1016/0022-5088(76)90057-6
138. Afzal M, Gupta N, Mallik A (2021) Experimental analysis of a metal hydride hydrogen storage system with hexagonal honeycomb-based heat transfer enhancements—part B. *Int J Hydrogen Energy* 46: 13131–13141. https://doi.org/10.1016/j.ijhydene.2020.11.275
139. Oi T, Maki K, Sakaki Y (2004) Heat transfer characteristics of the metal hydride vessel based on the plate-fin type heat exchanger. *J Power Sources* 125: 52–61. https://doi.org/10.1016/S0378-7753(03)00822-X
140. Mazzucco A, Dornheim M, Sloth M, et al. (2014) Bed geometries, fueling strategies and optimization of heat exchanger designs in metal hydride storage systems for automotive applications: A review. *Int J Hydrogen Energy* 39: 17054–17074. https://doi.org/10.1016/j.ijhydene.2014.08.047
141. Prasad JS, Muthukumar P (2023) Design of metal hydride reactor for medium temperature thermochemical energy storage applications. *Therm Sci Eng Prog* 37: 101570. https://doi.org/10.1016/j.tsep.2022.101570
142. El Mghari H, Huot J, Xiao J (2019) Analysis of hydrogen storage performance of metal hydride reactor with phase change materials. *Int J Hydrogen Energy* 44: 28893–28908. https://doi.org/10.1016/j.ijhydene.2019.09.090
143. Ye Y, Lu J, Ding J, et al. (2020) Numerical simulation on the storage performance of a phase change materials based metal hydride hydrogen storage tank. *Appl Energy* 278: 115682. https://doi.org/10.1016/j.apenergy.2020.115682
144. Zhou Y, Dong ZY, Hsieh WP, et al. (2022) Thermal conductivity of materials under pressure. *Nat Rev Phys* 4: 319–335. https://doi.org/10.1038/s42254-022-00423-9

145. Holman JP (2010) Heat Transfer, 10th ed. McGraw Hill Higher Education. Available from: https://books.google.co.za/books?id=I4M4TZ0h1FwC
146. Calise F, d'Accadia MD, Santarelli M, et al. (2019) *Solar Hydrogen Production: Processes, Systems and Technologies*. https://doi.org/10.1016/C2017-0-02289-9
147. Rana S, Monder DS, Chatterjee A (2024) Thermodynamic calculations using reverse Monte Carlo: A computational workflow for accelerated construction of phase diagrams for metal hydrides. *Comput Mater Sci* 233: 112727. https://doi.org/10.1016/j.commatsci.2023.112727
148. Ye Y, Yue Y, Lu J, et al. (2021) Enhanced hydrogen storage of a $LaNi_5$ based reactor by using phase change materials. *Renewable Energy* 180: 734–743. https://doi.org/10.1016/j.renene.2021.08.118
149. Wei TY, Lim KL, Tseng YS, et al. (2017) A review on the characterization of hydrogen in hydrogen storage materials. *Renewable Sustainable Energy Rev* 79: 1122–1133. https://doi.org/10.1016/j.rser.2017.05.132
150. Darzi AAR, Afrouzi HH, Moshfegh A (2016) Absorption and desorption of hydrogen in long metal hydride tank equipped with phase change material jacket. *Int J Hydrogen Energy* 41: 9595–9610. https://doi.org/10.1016/j.ijhydene.2016.04.051
151. Liu G, Li S, Song C, et al. (2024) High-entropy Ti-Zr-Hf-Ni-Cu alloys as solid-solid phase change materials for high-temperature thermal energy storage. *Intermetallic* 166: 108177. https://doi.org/10.1016/j.intermet.2023.108177
152. Jiang M, Yang Y, Li H, et al. (2024) Theoretical study on the surface poisoning of high-entropy alloys during hydrogen storage cycles: The effect of metal elements and phases. *Phys Chem Chem Phys* 26: 24384–24394. https://doi.org/10.1039/D4CP02831G
153. Kozhakhmetov Y, Skakov M, Kurbanbekov S, et al. (2025) High-Entropy alloys: Innovative materials with unique properties for hydrogen storage and technologies for their production. *Metals* 15: 100. https://doi.org/10.3390/met15020100
154. Liu F, Xiao L, Zhou R, et al. (2025) Evaluation of thermal stress and performance for solid oxide electrolysis cells employing graded fuel electrodes. *Energies* 18: 2790. https://doi.org/10.3390/en18112790
155. Kaushik M (2022) *Fundamentals of gas dynamics*. Singapore: Springer, 375–583. https://doi.org/10.1007/978-981-16-9085-3
156. Zhang Y, Wang H, Yang J, et al. (2025) Enhancing the strain-hardening rate and uniform tensile ductility of lightweight refractory high-entropy alloys by tailoring multi-scale heterostructure strategy. *Int J Plast* 185: 104237. https://doi.org/10.1016/j.ijplas.2024.104237
157. Chang SY, Li CE, Huang YC, et al. (2014) Structural and thermodynamic factors of suppressed interdiffusion kinetics in multi-component high-entropy materials. *Sci Rep*, 4. https://doi.org/10.1038/srep04162
158. Bouzidi A, Laversenne L, Zepon G, et al. (2021) Hydrogen sorption properties of a novel refractory Ti-V-Zr-Nb-Mo high entropy alloy. *Hydrogen* 2: 399–413. https://doi.org/10.3390/hydrogen204002
159. Dornheim M, Ling S, Stavila V (2025) Promising alloys for hydrogen storage in the compositional space of $(TiVNb)_{100-x}(Cr, Mo)_x$ high-entropy alloys. *ACS Appl Mater Interfaces* 17: 41991–42003. https://doi.org/10.1021/acsami.5c08574
160. Luo L, Chen L, Li L, et al. (2024) High-entropy alloys for solid hydrogen storage: A review. *Int J Hydrogen Energy* 50: 406–430. https://doi.org/10.1016/j.ijhydene.2023.07.146

161. Babaie Rizvandi O, Frandsen HL, Hendriksen PV (2022) Stack-Scale modeling of ammonia-fueled solid oxide fuel cell. *Meet Abstr* 241: 1960–1960. https://doi.org/10.1149/MA2022-01461960mtgabs
162. Pineda-Romero N, Perrière L, Elkaim E, et al. (2024) Advancing our understanding of the effect of Al/Mo substitution in the TiVNb alloy on the hydrogen storage properties. *J Alloys Compd* 1005: 176255. https://doi.org/10.1016/j.jallcom.2024.176255
163. Chen YT, Chang YJ, Murakami H, et al. (2020) Designing high entropy superalloys for elevated temperature application. *Scr Mater* 187: 177–182. https://doi.org/10.1016/j.scriptamat.2020.06.002
164. Zhao AZ, Garay JE (2023) High temperature liquid thermal conductivity: A review of measurement techniques, theoretical understanding, and energy applications. *Prog Mater Sci* 139: 101180. https://doi.org/10.1016/j.pmatsci.2023.101180
165. Mehrtash M, Tari I (2013) A correlation for natural convection heat transfer from inclined plate-finned heat sinks. *Appl Therm Eng* 51: 1067–1075. https://doi.org/10.1016/j.applthermaleng.2012.10.043
166. Wang H, Prasad AK, Advani SG (2012) Hydrogen storage systems based on hydride materials with enhanced thermal conductivity. *Int J Hydrogen Energy* 37: 290–298. https://doi.org/10.1016/j.ijhydene.2011.04.096
167. Shimizu Y, Nomura T (2023) Al–Si–Fe alloy-based phase change material for high-temperature thermal energy storage. *High Temp Mater Process*, 42. https://doi.org/10.1515/htmp-2022-0280
168. Kukkapalli VK, Kim S, Thomas SA (2023) Thermal management techniques in metal hydrides for hydrogen storage applications: A review. *Energies* 16: 3444. https://doi.org/10.3390/en16083444
169. Ding Z, Li Y, Jiang H, et al. (2025) The integral role of high-entropy alloys in advancing solid-state hydrogen storage. *Interdiscip Mater* 4: 75-108.https://doi.org/10.1002/idm2.12216
170. Cavaliere P (2025) Hydrogen embrittlement: The case of high-entropy alloys. *Hydrogen Embrittlement Met Alloys*, 681–728. https://doi.org/10.1007/978-3-031-83681-7_10
171. Andrade G, Huot J, Floriano R (2025) Microstructural evolution and hydrogen storage performance of TiZrHfVNb1-xCux (for X = 0, 0.6, 0.8 and 1) high-entropy alloys. *Mater Chem Phys* 343: 131069. https://doi.org/10.1016/j.matchemphys.2025.131069
172. Luo L, Han H, Feng D, et al. (2024) Nanocrystalline high entropy alloys with ultrafast kinetics and high storage capacity for large-scale room-temperature-applicable hydrogen storage. *Renewables* 2: 138–149. https://doi.org/10.31635/renewables.024.202300049
173. Sahlberg M, Karlsson D, Zlotea C, et al. (2016) Superior hydrogen storage in high entropy alloys. *Sci Rep* 6: 36770. https://doi.org/10.1038/srep36770
174. Ye Y, Zhu H, Cheng H, et al. (2023) Performance optimization of metal hydride hydrogen storage reactors based on PCM thermal management. *Appl Energy* 338: 120923. https://doi.org/10.1016/j.apenergy.2023.120923
175. Wang H, Ma S, Zhao W, et al. (2025) Exceptionally low thermal conductivity in distorted high entropy alloy. *Mater Res Lett* 13: 24–34. https://doi.org/10.1080/21663831.2024.2413101.
176. Steiner T (2002) The hydrogen bond in the solid state. *Angew Chem* 41: 48–76. https://doi.org/10.1002/1521-3773(20020104)41:1<48::AID-ANIE48>3.0.CO;2-U

177. Harrison WA (2012) Electronic structure and the properties of solids: The physics of the chemical bond. *Courier Corporation*, NY: Dover Publication. Available from: https://openlibrary.org/books/OL21680979M/Electronic_structure_and_theproperties_of_solids.
178. Pandey AK, Dixit CK, Srivastava S (2024) Theoretical model for the prediction of lattice energy of diatomic metal halides. *Math Chem* 62: 269–274. https://doi.org/10.1007/s10910-023-01538-9
179. Gong J, Li Y, Song X, et al. (2024) Hydrogen storage of high entropy alloy NbTiVZr and its effect on mechanical properties: A first-principles study. *Vacuum* 219: 112754. https://doi.org/10.1016/j.vacuum.2023.112754
180. Huang LA, Xu Y, Song Y, et al. (2024) Local electronic structure engineering of vanadium-doped nickel phosphide nanosheet arrays for efficient hydrogen evolution. *J Colloid Interface Sci* 658: 383–391. https://doi.org/10.1016/j.jcis.2023.12.049
181. Müller PC, Ertural C, Hempelmann J, et al. (2021) Crystal orbital bond index: Covalent bond orders in solids. *J Phys Chem C* 125: 7959–7970. https://doi.org/10.1021/acs.jpcc.1c00718
182. Marqués M, Peña-Alvarez M, Martínez-Canales M, et al. (2023) H_2 chemical bond in a high-pressure crystalline environment. *J Phys Chem C* 127: 15523–15532. https://doi.org/10.1021/acs.jpcc.3c02366
183. Osman AI, Ayati A, Farrokhi M, et al. (2024) Innovations in hydrogen storage materials: synthesis, applications, and prospects. *J Energy Storage* 95: 112376. https://doi.org/10.1016/j.est.2024.112376
184. Santis GD, Xantheas SS (2025) Extending Badger's rule. I. The relationship between energy and structure in hydrogen bonds. *J Chem Phys* 162: 044106 https://doi.org/10.1063/5.0244238
185. Yadav YK, Shaz MA, Yadav TP (2025) Solid-state hydrogen storage properties of Al–Cu–Fe–Ni–Ti high entropy alloy. *Int J Hydrogen Energy* 99: 985–995. https://doi.org/10.1016/j.ijhydene.2024.12.254
186. Aghdasi P, Li DY (2025) Electron work function guided tailoring of (W_{4-x}, Mx)C_4/doped Ni matrix interfacial bonding: Insights from first-principles calculations. *Acta Mater* 283: 120511. https://doi.org/10.1016/j.actamat.2024.120511
187. Savin A, Nesper R, Wengert S, et al. (1997) ELF: The electron localization function. *Angew Chemie* 36: 1808–1832. https://doi.org/10.1002/anie.199718081
188. Du Z, Zuo J, Bao N, et al. (2019) Effect of Ta addition on the structural, thermodynamic and mechanical properties of CoCrFeNi high entropy alloys. *RSC Adv* 9: 16447–16454. https://doi.org/10.1039/C9RA03055G
189. Bao N, Zuo J, Du Z (2019) Computational characterization of the structural and mechanical properties of $Al_xCoCrFeNiTi_{1-x}$ high entropy alloys. *Mater Res Express* 6: 096519. https://doi.org/10.1088/2053-1591/ab2b77
190. Zhang A, Zhao R, Wang Y, et al. (2023) Regulating the electronic structure of manganese-based materials to optimize the performance of zinc-ion batteries. *Energy Environ Sci* 16: 3240–3301. https://doi.org/10.1039/D3EE01344H
191. Cao FH, Wang YJ, Dai LH (2020) Novel atomic-scale mechanism of incipient plasticity in a chemically complex CrCoNi medium-entropy alloy associated with inhomogeneity in local chemical environment. *Acta Mater* 194: 283–294. https://doi.org/10.1039/D3EE01344H
192. Kumar S, Jain A, Ichikawa T, et al. (2017) Development of vanadium based hydrogen storage material: A review. *Renewable Sustainable Energy Rev* 72: 791–800. https://doi.org/10.1016/j.rser.2017.01.063

193. Anikina EY, Verbetsky VN (2021) Thermodynamic aspects of the reversible absorption of hydrogen by $Ti_{0.9}Zr_{0.1}Mn_{1.4}V_{0.5}$ alloy. *Russ J Phys Chem A* 95: 861–867. https://doi.org/10.1134/S0036024421050022
194. Yu J, Horsfield A (2025) Tight binding simulation of the MgO and $Mg(OH)_2$ hydration and carbonation processes. *J Chem Theory Comput* 21: 1961–1977. https://doi.org/10.1021/acs.jctc.4c01531
195. Hong Z, Wang L, Zhang W, et al. (2022) Hydrogen isotope permeation behavior of AlCrFeTiNb, AlCrMoNbZr and AlCrFeMoTi high-entropy alloys coatings. *Coatings* 12: 171. https://doi.org/10.3390/coatings12020171
196. Matczak P (2025) Quantum chemical topological analysis of [2Fe2S] core in novel [FeFe]-hydrogenase mimics. *Crystals* 15: 52. https://doi.org/10.3390/cryst15010052
197. Zhang JW, Zhou PP, Cao ZM, et al. (2023) Composition and temperature influence on hydrogenation performance of $TiZrHfMo_xNb_{2-x}$ high entropy alloys. *J Mater Chem A* 11: 20623–20635. https://doi.org/10.1039/D3TA01990J
198. Muthukumar P, Kumar A, Raju NN, et al. (2018) A critical review on design aspects and developmental status of metal hydride based thermal machines. *Int J Hydrogen Energy* 43: 17753–17779. https://doi.org/10.1016/j.ijhydene.2018.07.157
199. Baranowski B (1993) A simplified quantitative approach to the isothermal hysteresis in metallic hydrides with coherent interphases. *J Alloys Compd* 200: 87–92. https://doi.org/10.1016/0925-8388(93)90476-4
200. Speer JG, Matlock DK, DeCooman BC, et al. (2005) Comments on "On the definitions of paraequilibrium and orthoequilibrium" by M. Hillert and J. Agren, scripta materialia, 50: 697–9 (2004). *Scr Mater* 52: 83–85. https://doi.org/10.1016/j.scriptamat.2004.08.029
201. Oates WA, Flanagan TB (1983) On the origin of increasing hydrogen pressures in the two solid phase regions of intermetallic compound-hydrogen systems. *Scr Metall* 17: 983–986. https://doi.org/10.1016/0036-9748(83)90435-0
202. Zepon G, Silva BH, Zlotea C, et al. (2021) Thermodynamic modelling of hydrogen-multicomponent alloy systems: Calculating pressure-composition-temperature diagrams. *Acta Mater* 215: 117070. https://doi.org/10.1016/j.actamat.2021.117070
203. Osman AI, Nasr M, Mohamed AR, et al. (2024) Life cycle assessment of hydrogen production, storage, and utilization toward sustainability. *WIREs: Energy Environ* 13: 526. https://doi.org/10.1002/wene.526
204. Yang Z, Meng P, Jiang M, et al. (2024) Intermolecular hydrogen bonding networks stabilized organic supramolecular cathode for ultra-high capacity and ultra-long cycle life rechargeable aluminium batteries. *Angew Chem Int Ed* 63: e202403424. https://doi.org/10.1002/anie.202403424
205. Teng Y, Wang R, Sun X, et al. (2025) Composition screening and cycling degradation mechanisms of long-cycle-life superlattice hydrogen storage alloys. *J Alloys Compd* 1025: 180349. https://doi.org/10.1016/j.jallcom.2025.180349
206. Chen J, Li Z, Huang H, et al. (2022) Superior cycle life of TiZrFeMnCrV high entropy alloy for hydrogen storage. *Scr Mater* 212: 114548. https://doi.org/10.1016/j.scriptamat.2022.114548
207. Purdy G, Ågren J, Borgenstam A, et al. (2011) ALEMI: A ten-year history of discussions of alloying-element interactions with migrating interfaces. *Metall Mater Trans A* 42: 3703–3718. https://doi.org/10.1007/s11661-011-0766-0

208. Ponsoni JB, Balcerzak M, Botta WJ, et al. (2023) A comprehensive investigation of the $(Ti_{0.5}Zr_{0.5})_1(Fe_{0.33}Mn_{0.33}Cr_{0.33})_2$ multicomponent alloy for room-temperature hydrogen storage designed by computational thermodynamic tools. *J Mater Chem A* 11: 14108–14118. https://doi.org/10.1039/D3TA02197A
209. Gill SPA (2022) Thermodynamics, kinetics and microstructure modelling. *IOP Publishing*. https://doi.org/10.1088/978-0-7503-3147-0
210. Pelton AD, Koukkari P, Pajarre R, et al. (2014) Para-equilibrium phase diagrams. *J Chem Thermodyn* 72: 16–22. https://doi.org/10.1016/j.jct.2013.12.023
211. Strozi RB, Silva BH, Leiva DR, et al. (2023) Tuning the hydrogen storage properties of Ti-V-Nb-Cr alloys by controlling the Cr/(TiVNb) ratio. *J Alloys Compd* 932: 167609. https://doi.org/10.1016/j.jallcom.2022.167609
212. Ling H, Tang Y, Zhong J, et al. (2025) Thermodynamic, diffusion and precipitation behaviors in Cu–Ni–Si–Co alloys: Modeling and experimental validation. *J Mater Res Technol* 35: 3257–3269. https://doi.org/10.1016/j.jmrt.2025.01.242
213. Pedroso OA, Botta WJ, Zepon G (2022) An open-source code to calculate pressure-composition-temperature diagrams of multicomponent alloys for hydrogen storage. *Int J Hydrogen Energy* 47: 32582–32593. https://doi.org/10.1016/j.ijhydene.2022.07.179
214. Massimino F (2012) Analysis of inhomogeneities in hydrogen storage alloys: A comparison of different methods. *Cryst Struct Theory Appl* 1: 100–106. https://doi.org/10.4236/csta.2012.13019
215. Lee JH, Ha SV, Seong J, et al. (2025) Development of 3D interconnected nanoporous TiZrHfNbTaNi high-entropy alloy via liquid metal dealloying and subsequent synthesis of (TiZrHfNbTaNi) O high-entropy oxide. *J Mater Res Technol* 35: 5204–5215 https://doi.org/10.1016/j.jmrt.2025.02.152
216. Al Zoubi W, Putri RAK, Abukhadra MR, et al. (2023) Recent experimental and theoretical advances in the design and science of high-entropy alloy nanoparticles. *Nano Energy* 110: 108362. https://doi.org/10.1016/j.nanoen.2023.108362
217. Nygård MM, Ek G, Karlsson D, et al. (2019) Counting electrons—A new approach to tailor the hydrogen sorption properties of high-entropy alloys. *Acta Mater* 175: 121–129. https://doi.org/10.1016/j.actamat.2019.06.002
218. Kumar A, Yadav TP, Shaz MA, et al. (2024) Hydrogen storage properties in rapidly solidified TiZrVCrNi high-entropy alloys. *Energy Storage* 6: e532. https://doi.org/10.1002/est2.532
219. Strozi RB, Witman M, Stavila V, et al. (2023) Elucidating primary degradation mechanisms in high-cycling-capacity, compositionally tunable high-entropy hydrides. *ACS Appl Mater Interfaces* 15: 38412–38422. https://doi.org/10.1021/acsami.3c05206
220. Ryltsev RE, Estemirova SK, Gaviko VS, et al. (2022) Structural evolution in TiZrHfNb high-entropy alloy. *Materialia* 21: 101311. https://doi.org/10.1016/j.mtla.2021.101311
221. Yan X, Zhang Y (2020) Functional properties and promising applications of high entropy alloys. *Scr Mater* 187: 188–193. https://doi.org/10.1016/j.scriptamat.2020.06.017
222. O'Connell JP, Haile JM (2005) *Thermodynamics: Fundamentals for applications*. 1 Eds., Cambridge University Press, 1–654. https://doi.org/10.1017/CBO9780511840234
223. Alaneme KK, Anaele JU, Kareem SA (2023) Hot deformability, microstructural evolution and processing map assessment of high entropy alloys: A systematic review. *J Mater Res Technol* 26: 1754–1784. https://doi.org/10.1016/j.jmrt.2023.07.242

224. Nguyen HQ, Shabani B (2021) Review of metal hydride hydrogen storage thermal management for use in the fuel cell systems. *Int J Hydrogen Energy* 46: 31699–31726. https://doi.org/10.1016/j.ijhydene.2021.07.057
225. Ozawa T (2000) Thermal analysis—Review and prospect. *Thermochim Acta* 355: 35–42. https://doi.org/10.1016/S0040-6031(00)00435-4
226. Kissinger HE (1957) Reaction kinetics in differential thermal analysis. *Anal Chem* 29: 1702–1706. https://doi.org/10.1021/ac60131a045
227. Vyazovkin S, Koga N, Schick C (2018) Handbook of thermal analysis and calorimetry recent advances, techniques and applications. 2 Eds, *Netherlands, Elsevier Science*, 1–842. Available from: https://searchworks.stanford.edu/view/13119808
228. Li X, Yin J, Zhang J, et al. (2022) Hydrogen embrittlement and failure mechanisms of multi-principal element alloys: A review. *J Mater Sci Technol* 122: 20–32. https://doi.org/10.1016/j.jmst.2022.01.008
229. Kong X, Jiang H, Lv Y, et al. (2025) Research progress on the hydrogen embrittlement resistance performance of high-entropy alloys. *Materials* 18: 2862. https://doi.org/10.3390/ma18122862
230. Balaji V, Jeyapandiarajan P, Joel J, et al. (2024) Mitigating hydrogen embrittlement in high-entropy alloys for next-generation hydrogen storage systems. *J Mater Res Technol* 33: 7681–7697. https://doi.org/10.1016/j.jmrt.2024.11.139
231. Tasan CC (2022) New tools & new insights: Unravelling hydrogen effects in structural alloys. *Microsc Microanal* 28: 1600. https://doi.org/10.1017/S1431927622006407
232. Chen YS, Huang C, Liu PY, et al. (2025) Hydrogen trapping and embrittlement in metals—A review. *Int J Hydrogen Energy* 136: 789–821. https://doi.org/10.1016/j.ijhydene.2024.04.076
233. Zhou X, Tehranchi A, Curtin WA (2021) Mechanism and prediction of hydrogen embrittlement in FCC stainless steels and high entropy alloys. *Phys Rev Lett* 127: 175501. https://doi.org/10.1103/PhysRevLett.127.175501
234. Padmanabhan NT, Clarizia L, Ganguly P (2025) Advancing hydrogen storage: critical insights to potentials, challenges, and pathways to sustainability. *Curr Opin Chem Eng* 48: 101135. https://doi.org/10.1016/j.coche.2025.101135
235. Duarte MJ, Fang X, Rao J, et al. (2021) In situ nanoindentation during electrochemical hydrogen charging: a comparison between front-side and a novel back-side charging approach. *J Mater Sci* 56: 8732–8744. https://doi.org/10.1007/s10853-020-05749-2
236. Pandey S, Srivastava R, Narain R (2025) Integrated analysis of energy-process parameters relationship in direct energy deposition of 15–5 PH stainless steel. *Int J Interact Des Manuf* 19: 3593–3610. https://doi.org/10.1007/s12008-024-01998-6
237. Jiang W, Zhu Y, Zhao Y (2022) Mechanical properties and deformation mechanisms of heterostructured high-entropy and medium-entropy alloys: A review. *Front Mater* 8: 792359. https://doi.org/10.3389/fmats.2021.792359
238. Maier-Kiener V, Ebner AS, Clemens H, et al. (2019) Impact of temperature and hydrogen on the nanomechanical properties of a highly deformed high entropy alloy. *Nanomechanical Testing in Materials Research and Development VII. Jon Molina-Aldareguia*, IMDEA-Materials Institute, Spain Eds, ECI Symposium Series. Available from: https://dc.engconfintl.org/nanochemtest_vii/107.
239. Feng Z, Li X, Song X, et al. (2022) Hydrogen embrittlement of CoCrFeMnNi high-entropy alloy compared with 304 and IN718 alloys. *Metals* 12: 998. https://doi.org/10.3390/met12060998

240. Huskova P, Horník J, Čižmárová E, et al. (2022) Metallic Materials for Hydrogen Storage—A Brief Overview. *Coatings* 12: 1813. https://doi.org/10.3390/coatings12121813
241. Muradyan G, Dolukhanyan S, Ter-Galstyan O, et al. (2025) The role of hydrogen in the synthesis of High-entropy alloys and their hydrides. *J Alloys Compd* 1010: 177327. https://doi.org/10.1016/j.jallcom.2024.177327
242. Bansal A, Kumar P, Yadav S, et al. (2023) Accelerated design of high entropy alloys by integrating high throughput calculation and machine learning. *J Alloys Compd* 960: 170543. https://doi.org/10.1016/j.jallcom.2023.170543
243. Jalali M, Nayebpashaee N (2025) A comprehensive review on the applications of high-entropy alloys in electronics and energy industries. *Fifth National and the First International Conference on Applied Research in Electrical Engineering (AREE)*, 1–5. https://doi.org/10.1109/AREE63378.2025.10880254
244. Bastin A, Robertson T, Durocher A, et al. (2025) Environmental resistance of high entropy alloys: Impact of downstream hydrogen combustion on oxidation resistance. *J Eng Gas Turbines Power* 148: 021020. https://doi.org/10.1115/1.4069580
245. Jiang Y, Jiang W (2024) High entropy alloys: emerging materials for advanced hydrogen storage. *Energy Technol* 12: 2401061. https://doi.org/10.1002/ente.202401061
246. Ma X, Ding X, Chen R, et al. (2022) Enhanced hydrogen storage properties of $ZrTiVAl_{1-x}$ Fe_x high-entropy alloys by modifying the Fe content. *RSC Adv* 12: 11272–11281. https://doi.org/10.1039/D2RA01064J

AIMS Press